

EDDA 1.0: integrated simulation of debris flow erosion, deposition and property changes

H. X. Chen¹ and L. M. Zhang¹

[1]{Department of Civil and Environmental Engineering, The Hong Kong University of
Science and Technology, Clear Water Bay, Hong Kong}

Correspondence to: L. M. Zhang (cezhangl@ust.hk)

Abstract

Debris flow material properties change during the initiation, transportation and deposition processes, which influences the runout characteristics of the debris flow. A quasi-three-dimensional depth-integrated numerical model, EDDA, is presented in this paper to simulate debris flow erosion, deposition and induced material property changes. The model considers changes in debris flow density, yield stress and dynamic viscosity during the flow process. The yield stress of the debris flow mixture determined at limit equilibrium using the Mohr-Coulomb equation is applicable to clear water flow, hyper-concentrated flow and fully developed debris flow. To assure numerical stability and computational efficiency at the same time, an adaptive time stepping algorithm is developed to solve the governing differential equations. Four numerical tests are conducted to validate the model. The first two tests involve a one-dimensional debris flow with constant properties and a two-dimensional dam-break water flow. The last two tests involve erosion and deposition, and the movement of multi-directional debris flows. The changes in debris flow mass and properties due to either erosion or deposition are shown to affect the runout characteristics significantly. The model is also applied to simulate a large-scale debris flow in Xiaojiagou Ravine to test the performance of the model in catchment-scale simulations. The results suggest that the model estimates well the volume, inundated area, and runout distance of the debris flow. The model is intended for use as a module in a real-time debris flow warning system.

1 **1 Introduction**

2 Debris flow is a flow of a sediment-water mixture driven by gravity. The mechanical triggers
3 of debris flows can be classified into three types; namely, erosion by surface runoff,
4 transformation from landslides, and collapse of debris dams (Takahashi, 2007). Basal erosion,
5 side erosion, and any other surficial material entrainment during the marching process entrain
6 additional material into the flow; the final volume can be several or dozens times of the initial
7 volume (e.g. Hungr et al., 2005; Chen et al., 2006; Berger et al., 2010; Chen et al., 2012; Chen
8 et al., 2014a). When the debris flow moves to a flatter area, the coarse materials can deposit
9 gradually. During the entire movement process, not only the debris flow volume, flow
10 velocity and flow depth change significantly, the properties of the debris flow mixture also
11 change substantially, which in turn influence the runout characteristics.

12 The mechanisms of changes in debris flow mass are important and have attracted the attention
13 of many researchers (e.g. Cannon and Savage, 1988; Takahashi et al., 1992; Hungr, 1995;
14 Egashira et al., 2001; Iverson, 2012). Cannon and Savage (1988) and Hungr (1995) proposed
15 one-dimensional lumped-mass models based on momentum conservation to describe the
16 entrainment or loss of material during the movement of a debris flow. Takahashi et al. (1992)
17 proposed a model to describe erosion and deposition based on volumetric sediment
18 concentration and flow velocity. Researchers have also described the erosion process from a
19 stress point of view (e.g. Medina et al., 2008; Iverson, 2012; Quan Luna et al., 2012): erosion
20 occurs when the basal shear stress exceeds the critical erosive shear stress of the bedding
21 material.

22 During the entire process of a debris flow, the debris flow properties can change significantly.
23 The volumetric sediment concentration (i.e. ratio of the solid volume to the total volume of
24 the debris flow mixture) can increase substantially due to entrainment of solid materials (e.g.
25 Takahashi et al., 1992; Egashira et al., 2001) or decrease due to deposition (e.g. Takahashi et
26 al., 1992) and dilution (e.g. Pierson and Scott, 1985). Accordingly, the rheological
27 characteristics of debris flows (e.g. yield stress and dynamic viscosity) will change with the
28 volumetric sediment concentration, which has been observed in a large number of
29 experiments (e.g. O'Brien and Julien, 1988; Rickenmann, 1991; Major and Pierson, 1992;
30 Sosio and Crosta, 2009; Bisantino et al., 2010). Various rheological models have been
31 adopted to describe debris flows, such as the laminar flow model (e.g. Takahashi, 2007), the

1 Bingham fluid model (e.g. Fraccarollo and Papa, 2000), the Voellmy model (e.g. Medina et
2 al., 2008), and the quadratic rheological model (Julien and Lan, 1991).

3 Based on understanding of erosion, deposition and rheology of debris flow materials, great
4 efforts have been made to simulate the movement of debris flows (e.g. Cannon and Savage,
5 1988; Takahashi et al., 1992; Hungr, 1995; Denlinger and Iverson, 2001; Ghilardi et al., 2001;
6 Chen et al., 2006; Pastor et al., 2009; Li et al., 2012; Chen et al., 2013; van Asch et al., 2014).
7 The numerical methods include the finite difference method (e.g. Takahashi et al., 1992), the
8 finite volume method (e.g. Medina et al., 2008), the finite element method (e.g. Crosta et al.,
9 2003), the distinct element method (e.g. Li et al., 2012), the smoothed particle hydrodynamics
10 method (e.g. Pastor et al., 2009) and others. Several computer programs have been written for
11 debris flow analysis, such as DAMBRK (Boss Corporation, 1989), FLO-2D (O'Brien et al.,
12 1993), DAN (Hungr, 1995), TOCHNOG (Crosta et al., 2003), 3dDMM (Kwan and Sun,
13 2006), FLATModel (Medina et al., 2008), DAN3D (Hungr and McDougall, 2009),
14 MassMov2D (Beguer á et al., 2009), PASTOR (Pastor et al., 2009), and RAMMS (Bartelt et
15 al., 2013).

16 Depth-integrated models have been widely adopted to describe erosion and deposition (e.g.
17 Takahashi et al., 1992; McDougall and Hungr, 2005; Armanini et al., 2009; Hungr and
18 McDougall, 2009; Iverson et al., 2011; Quan Luna et al., 2012; Ouyang et al., 2014). The
19 Mohr-Coulomb failure process was adopted to simulate bed erosion (e.g. Medina et al., 2008;
20 Quan Luna et al., 2012). Ouyang et al. (2014) further combined the Mohr-Coulomb model
21 and the Voellmy model to overcome the flaws of each of these two models. The changes in
22 flow depth, flow velocity and debris mass have been accounted for in the literature. Limited
23 attempt has also been made to consider the evolution of volumetric sediment concentration
24 (Takahashi et al., 1992; Denlinger and Iverson, 2001; Ghilardi et al., 2001). Several key
25 problems, however, still remain. How can one describe the various phases of a debris flow
26 (e.g. clear water flow, hyper-concentrated flow, and fully developed debris flow) using a
27 general rheological model? How do the properties of debris flows (e.g. volumetric sediment
28 concentration, yield stress, viscosity) change in the erosion and deposition processes? How do
29 these changes affect the runout characteristics of the debris flow? These problems are very
30 important for the risk assessment of debris flows.

31 The objective of this paper is to develop a numerical model to consider the erosion and
32 deposition processes and debris flow property changes during these processes. The paper is

1 organized as follows. The methodology is introduced in Sect. 2, including the problem
2 description, governing equations, constitutive models, initiation of erosion and deposition,
3 numerical solution algorithm, time stepping and numerical stability. The model is tested and
4 verified in Sect. 3 using analytical solution, numerical solutions, and experimental tests. A
5 large-scale debris flow event in the Wenchuan earthquake zone is simulated as a field
6 application in Sect. 4. The limitations of the model are indicated in Sect. 5.

7 **2 Methodology**

8 **2.1 Problem description**

9 The volume of a debris flow can increase due to erosion or entrainment and decrease due to
10 deposition. Due to changes in sediment concentration, a debris flow triggered by surface
11 runoff may experience several flow regimes. The debris flow can evolve from a clear water
12 flow to a hyper-concentrated flow, a fully developed debris flow, and finally a deposit on the
13 debris fan. The erosion and deposition processes and property changes in debris flow are
14 illustrated in Fig. 1. The debris flow entrains and incorporates materials from the channel bed
15 if the volumetric sediment concentration, C_v , is smaller than an equilibrium value, $C_{v\infty}$, for the
16 channel gradient and the shear stress is sufficiently large. Some material separates from the
17 debris flow mixture and deposits on the channel bed when the volumetric sediment
18 concentration is larger than an equilibrium value for the channel gradient and the flow
19 velocity is not sufficient to take all the material. Due to erosion and deposition, debris flow
20 properties change significantly. The changes in the volumetric sediment concentration, yield
21 stress and viscosity are shown in Fig. 2 and Fig. 3. When it is a clear water flow, only a small
22 amount of solid particles moves with the flow. The yield stress is negligible, and the dynamic
23 viscosity is close to that of water. When solid materials are entrained into the flow due to
24 erosion, the flow may evolve into a hyper-concentrated flow. The flow develops a significant
25 yield stress, and the dynamic viscosity increases to a certain level. A debris flow can fully
26 develop after sufficient solid materials are entrained into the flow. The yield stress and
27 dynamic viscosity increase to relatively high levels. The debris flow will decelerate when
28 moving to a flatter area, and deposition occurs along the flow path. The volumetric sediment
29 concentration hence decreases in the deposition process.

1 2.2 Governing differential equations

2 In this study, an integrated numerical model is developed to simulate debris flow erosion,
 3 deposition, and the induced property changes. The model is named as EDDA, which stands
 4 for erosion (E)-deposition (D) debris flow analysis (DA). The reference frame is defined in
 5 Fig. 1. Depth-integrated mass conservation equations (Eqs. 1 and 2) and momentum
 6 conservation equations (Eqs. 3 and 4) are adopted to describe the movement of a debris flow:

$$7 \frac{\partial h}{\partial t} + \frac{\partial(hv_x)}{\partial x} + \frac{\partial(hv_y)}{\partial y} = i[C_{v^*} + (1 - C_{v^*})s_b] + A[C_{vA} + (1 - C_{vA})s_A], \quad (1)$$

$$8 \frac{\partial(C_v h)}{\partial t} + \frac{\partial(C_v h v_x)}{\partial x} + \frac{\partial(C_v h v_y)}{\partial y} = iC_{v^*} + AC_{vA}, \quad (2)$$

$$9 \frac{\partial v_x}{\partial t} + v_x \frac{\partial v_x}{\partial x} = g \left[-\text{sgn}(v_x) S_{fx} - \frac{\partial(z_b + h)}{\partial x} \right] - \frac{v_x \{i[C_{v^*} + (1 - C_{v^*})s_b] + A[C_{vA} + (1 - C_{vA})s_A]\}}{h}, \quad (3)$$

$$11 \frac{\partial v_y}{\partial t} + v_y \frac{\partial v_y}{\partial y} = g \left[-\text{sgn}(v_y) S_{fy} - \frac{\partial(z_b + h)}{\partial y} \right] - \frac{v_y \{i[C_{v^*} + (1 - C_{v^*})s_b] + A[C_{vA} + (1 - C_{vA})s_A]\}}{h}, \quad (4)$$

13 where h is the flow depth; t is time; v_x and v_y are the depth-averaged flow velocity in x and y
 14 directions, respectively; i is the erosion rate (> 0) or deposition rate (< 0); A is the rate of
 15 surficial material entrainment from collapse of bank materials or detached landslide materials;
 16 C_{v^*} and C_{vA} are the volume fraction of solids in the erodible bed and the entrained surficial
 17 materials, respectively; s_b and s_A are the degree of saturation of the erodible bed and entrained
 18 surficial materials, respectively; C_v is the volumetric sediment concentration of the debris
 19 flow mixture; g is the gravitational acceleration; S_{fx} and S_{fy} are the flow resistance slopes in x
 20 and y directions, respectively; z_b is the bed elevation; the sgn (i.e. signum) function is used to
 21 make sure the direction of the flow resistance is opposite to that of the flow direction.

22 Similar to the two-dimensional model proposed by O'Brien et al. (1993), the governing
 23 equations above use a global coordinate system, which has been proven to simulate well
 24 flows in channels and alluvial fans (Akan and Yen, 1981; O'Brien et al., 1993). The
 25 difference is that EDDA considers changes in debris flow properties due to material
 26 entrainment and the induced momentum exchange. In Eqs. (3) and (4), the flow velocity
 27 gradient in the orthogonal direction is neglected, since very little accuracy is sacrificed by

1 neglecting this term (Akan and Yen, 1981; O'Brien et al., 1993). In this study, erosion and
2 deposition are investigated while surficial material entrainment is not. The bed elevation
3 changes in the erosion and deposition processes, and can be expressed as

$$4 \quad \frac{\partial z_b}{\partial t} = -i. \quad (5)$$

5 **2.3 Constitutive models**

6 Various forms of rheological models can be implemented in the momentum conservation
7 equation, which allows the simulation of various types of flows. Several most widely used
8 rheological models are introduced below to compute S_f ; namely, the laminar flow model, the
9 turbulent flow model, the Bingham fluid model, the Voellmy model, and the quadratic
10 rheological model.

11 The laminar flow model is useful to describe the movement of a fully liquefied flow, which is
12 governed by viscous behaviour. The flow resistance slope is expressed as

$$13 \quad S_f = \frac{3\mu V}{\rho g h^2}, \quad (6)$$

14 where μ is the dynamic viscosity; V is the absolute value of depth-averaged flow velocity; ρ is
15 the debris flow density; g is the gravitational acceleration.

16 Turbulent flows with low volumetric sediment concentration are often analysed using the
17 Manning equation:

$$18 \quad S_f = \frac{n^2 V^2}{h^{4/3}}, \quad (7)$$

19 where n is the Manning coefficient.

20 The Bingham fluid model considers both plastic and viscous behaviours. A Bingham fluid
21 does not move if the shear stress is smaller than a threshold yield stress, but behaves as a
22 viscous material when the shear stress exceeds the threshold. The model is expressed as

$$23 \quad S_f = \frac{\tau_0}{\rho g h}, \quad (8)$$

24 where

$$2\tau_0^3 - 3(\tau_y + 2\frac{\mu V}{h})\tau_0^2 + \tau_y^3 = 0, \quad (9)$$

where τ_0 is the basal shear stress; τ_y is the yield stress of debris flow.

The Voellmy model (Voellmy, 1955) combines the effects of frictional and turbulent behaviours:

$$S_f = \cos \theta \tan \phi + \frac{V^2}{\xi h}, \quad (10)$$

where θ is the bed slope; ϕ is the friction angle of the solid particles contacting the bed; ξ is a turbulence parameter.

The quadratic rheological model proposed by Julien and Lan (1991) considers the effects of frictional behaviour, viscous behaviour, and turbulent behaviour plus the resistance arising from solid-particle contacts, which are represented by three terms as follows:

$$S_f = \frac{\tau_y}{\rho gh} + \frac{K\mu V}{8\rho gh^2} + \frac{n_{td}^2 V^2}{h^{4/3}}, \quad (11)$$

where n_{td} is the equivalent Manning coefficient, which accounts for both the turbulent behaviour and the resistance arising from solid-particle contacts and is expressed as (FLO-2D Software Inc., 2009)

$$n_{td} = 0.0538ne^{6.0896C_v}. \quad (12)$$

Since the quadratic rheological model accounts for the most comprehensive flow behaviour, it is adopted into the governing differential equations in this paper.

O'Brien and Julien (1988) proposed the following empirical relationships to estimate the yield stress, τ_y , and the dynamic viscosity, μ , based on laboratory tests:

$$\tau_y = \alpha_1 e^{\beta_1 C_v}, \quad (13)$$

$$\mu = \alpha_2 e^{\beta_2 C_v}, \quad (14)$$

where α_1 , α_2 , β_1 and β_2 are empirical coefficients. The equations describe well the changes of τ_y and μ with C_v when the C_v value is sufficiently large. But for very small C_v values (e.g. 0 for water), Eqs. (13) and (14) give α_1 and α_2 , respectively, while in reality τ_y and μ are 0 and 0.001 Pa.s at 20°, respectively when C_v is 0. In this study, a new equation is derived to

1 estimate τ_y . Assuming a hydrostatic pressure distribution within the debris flow, the effective
2 normal stress on the inclined channel bed can be expressed as

$$3 \quad \sigma = C_v(\rho_s - \rho_w)gh \cos^2 \theta, \quad (15)$$

4 where ρ_s is the density of solid particles; ρ_w is the density of water; θ is the bed slope. If
5 suspension of particles is not considered, the yield stress at limit equilibrium can be calculated
6 using the Mohr-Coulomb equation:

$$7 \quad \tau_y = C_v(\rho_s - \rho_w)gh \cos^2 \theta \tan \phi, \quad (16)$$

8 where ϕ is the friction angle of the solid particles contacting the bed. The effective cohesion
9 of the debris flow material is taken as zero in the above equation. If only the particles in
10 contact are considered, the yield stress can be calculated by incorporating a coefficient of
11 suspension of solid particles as follows:

$$12 \quad \tau_y = (1 - C_s)C_v(\rho_s - \rho_w)gh \cos^2 \theta \tan \phi, \quad (17)$$

13 where C_s is the coefficient of suspension of solid particles and $(1 - C_s)$ represents the portion of
14 solid particles that are in contact.

15 Three typical suspension scenarios are shown in Fig. 4: partial suspension, $0 < C_s < 1$; full
16 suspension, $C_s = 1$; and no suspension, $C_s = 0$. The three scenarios have the same volumetric
17 sediment concentration but different C_s values. C_s is in the range between 0 and 1 in most
18 cases, which means that the solid particles are partly suspended (Fig. 4a). C_s is 1 when all the
19 solid particles are suspended and do not contact with the bed (Fig. 4b); C_s is 0 when all the
20 solid particles are retained on the bed and no suspension occurs (Fig. 4c). In reality, some of
21 the solid particles are in suspension due to buoyant forces, collision between solid particles,
22 and turbulent fluid forces. The value of C_s is related to particle size and flow discharge. A
23 smaller particle size gives a larger C_s value since smaller particles are more likely to suspend
24 in water. Larger flow discharges also give larger C_s values based on field observations
25 (Alexandrov et al., 2003).

26 Equation (17) is suitable for calculating the changing yield stress especially at low solid
27 concentrations. Equation (13) is suitable for calculating the changing yield stress especially at
28 high solid concentrations and performs well on alluvial fans (O'Brien et al., 1993). Therefore,
29 Eqs. (17) and (13) are adopted to calculate the yield stress in a confined channel with erodible

1 materials and an unconfined flat area, respectively. The combination of the two equations
 2 overcomes the drawbacks of each of the two equations.

3 The values of C_v in most laboratory tests range between 0.1 and 0.8 (e.g. O'Brien and Julien,
 4 1988; Coussot et al., 1998; Schatzmann et al., 2009; Sosio and Crosta, 2009; Bisantino et al.,
 5 2010) and Eq. (14) can be adopted to estimate μ when C_v is greater than or equal to 0.1. When
 6 C_v is smaller than 0.1, Eq. (14) is not valid and μ is assumed to increase linearly from 0.001
 7 Pa.s for water to $\alpha_2 e^{0.1\beta^2}$.

8 **2.4 Initiation of erosion and deposition**

9 Erosion occurs when the bed shear stress is sufficiently large and the volumetric sediment
 10 concentration is smaller than an equilibrium value. The equilibrium value proposed by
 11 Takahashi et al. (1992) is adopted in this study:

$$12 \quad C_{v\infty} = \frac{\rho_w \tan \theta}{(\rho_s - \rho_w)(\tan \phi_{bed} - \tan \theta)}, \quad (18)$$

13 where $C_{v\infty}$ is the equilibrium volumetric sediment concentration; ϕ_{bed} is the internal friction
 14 angle of the erodible bed. The computed $C_{v\infty}$ value is larger than 1 when θ approaches ϕ_{bed} ,
 15 and smaller than 0 when θ is larger than ϕ_{bed} , both indicating an unstable or quasi-stable bed.
 16 Solid materials are difficult to be retained on such a steep slope. Hence, no erosion is
 17 expected to occur on such a slope.

18 The erosion rate can be described approximately by the following equation:

$$19 \quad i = K_e(\tau - \tau_c), \quad (19)$$

20 where i is the erosion rate; K_e is the coefficient of erodibility, which is a soil property that
 21 describes the erosion speed; τ is the shear stress; τ_c is the critical erosive shear stress. The
 22 shear stress (Hanson, 1990) can be computed as follows:

$$23 \quad \tau = \rho g h S_f. \quad (20)$$

24 Medina et al. (2008) and Quan Luna et al. (2012) consider bed erosion as a Mohr-Coulomb
 25 failure process. In this study, the critical erosive shear stress can be calculated by considering
 26 the partly suspended particles at limit equilibrium using the Mohr-Coulomb equation:

$$27 \quad \tau_c = c' + (1 - C_s)C_v(\rho_s - \rho_w)gh \cos^2 \theta \tan \phi_{bed}, \quad (21)$$

1 where c' is the effective cohesion of the bed material. Based on Eqs. (18)-(21), erosion occurs
 2 if τ is larger than τ_c and C_v is smaller than $C_{v\infty}$ (Fig. 1). K_e and τ_c can also be measured in-situ
 3 using a jet index method (e.g. Chang et al., 2011).

4 When the debris flow moves to a flatter place, deposition occurs if C_v is larger than the
 5 respective $C_{v\infty}$ value (Fig. 1) and the flow velocity is smaller than a critical value. Takahashi
 6 et al. (1992) proposed the following critical flow velocity for the initiation of deposition:

$$7 \quad V_e = \frac{2}{5d_{50}} \left(\frac{g \sin \theta_e \rho}{0.02 \rho_s} \right)^{0.5} \lambda^{-1} h^{1.5}, \quad (22)$$

8 where

$$9 \quad \tan \theta_e = \frac{C_v (\rho_s - \rho_w) \tan \phi_{bed}}{C_v (\rho_s - \rho_w) + \rho_w}, \quad (23)$$

$$10 \quad \lambda^{-1} = \left(\frac{C_{v^*}}{C_v} \right)^{\frac{1}{3}} - 1, \quad (24)$$

11 ρ is the density of debris flow and can be computed as follows:

$$12 \quad \rho = C_v (\rho_s - \rho_w) + \rho_w, \quad (25)$$

13 where d_{50} is the mean particle size of the debris flow mixture. The deposition rate can be
 14 expressed as follows (Takahashi et al., 1992):

$$15 \quad i = \delta_d \left(1 - \frac{V}{pV_e} \right) \frac{C_{v\infty} - C_v}{C_{v^*}} V, \quad (26)$$

16 where δ_d is a coefficient that describes the deposition rate; p (<1) is a coefficient introduced to
 17 account for the difference between the locations where actual deposition takes place in the
 18 experiment and where the velocity becomes less than V_e (Takahashi et al., 1992), and a value
 19 of 0.67 is recommended by Takahashi et al. (1992).

20 **2.5 Numerical solution algorithm**

21 The analysis domain is discretized into a grid first, with properties of each cell assigned,
 22 including the initial flow depth, the thickness and properties of the erodible soil layer, the
 23 elevation of the non-erodible layer, Manning's coefficient and so on. As shown in Eqs. (1)
 24 and (2), the changes in h and C_v are governed by two effects; namely, erosion or deposition,

1 and the flow exchange among cells. The change in flow velocity is governed by four effects;
 2 namely, convective acceleration, flow resistance, total head, and momentum exchange due to
 3 erosion or deposition. A volume conservation algorithm is developed to describe the changes
 4 in debris flow properties and the movement of debris flow.

5 As shown in Fig. 5, each cell has eight flow directions; namely, four compass directions (i.e.
 6 north, east, south and west) and four diagonal directions (i.e. northeast, southeast, southwest
 7 and northwest). In each time step, the changes in h and C_v at each cell due to erosion or
 8 deposition are first evaluated. After that, the flow velocity, the flow discharge, and the density
 9 of the exchange flow across each flow boundary (i.e. $\Gamma_N, \Gamma_E, \Gamma_S, \Gamma_W, \Gamma_{NE}, \Gamma_{SE}, \Gamma_{SW}, \Gamma_{NW}$) of
 10 all the cells are computed; and the changes in h and C_v at each cell due to the flow exchange
 11 among the cells are then evaluated. The computation of the flow velocity in each of the eight
 12 directions is independent. Therefore, Eqs. (3) and (4) are reduced to one equation. This type
 13 of method has been proven to be sufficient and efficient for simulating overland flows (FLO-
 14 2D Software Inc., 2009). The numerical solution algorithm is introduced step by step as
 15 follows:

16 (1) At the beginning of each time step, the erosion rate or deposition rate is computed for
 17 each cell. The flow depth and volumetric sediment concentration of each cell are updated
 18 using Eqs. (1) and (2) as follows:

$$19 \quad h_{predi} = h^n + \{i[C_{v^*} + (1 - C_{v^*})s_b]\} \Delta t, \quad (27)$$

$$20 \quad C_{vpredi} = \frac{(C_v^n h^n + iC_{v^*} \Delta t)}{h_{predi}}, \quad (28)$$

21 where superscript n notes the sequence of time stepping. The spatial differences of h and
 22 $C_v h$ in Eqs. (1) and (2) are not considered at this stage but will be accounted for in step 4.
 23 The updated bed elevation and density of flow, ρ_{predi} , can be computed using Eqs. (5) and
 24 (25), respectively.

25 (2) At each flow boundary, the average flow depth, flow density, volumetric sediment
 26 concentration and roughness of the two cells bounded at the boundary are computed. The bed
 27 slope between the two cells is defined using the gradient between the centres of the cells.

1 (3) The new flow velocity across each flow boundary is obtained by solving the
2 momentum conservation equation:

$$3 \quad v_{predi} = v^n + \left\{ g \left[-\text{sgn}(v^n) S_f - \frac{\partial(z_b + h_{predi})}{\partial x} \right] - \frac{v^n i [C_{v^*} + (1 - C_{v^*}) s_b]}{h_{predi}} - v^n \frac{\partial v^n}{\partial x} \right\} \Delta t, \quad (29)$$

4 (4) The discharge, q , across the flow boundaries is then computed, and the flow depth and
5 density at a cell are updated as follows:

$$6 \quad h_{new} = h_{predi} + \frac{\sum_{b=1}^{nb} (q_b \Delta t)}{A_{cell}}, \quad (30)$$

$$7 \quad \rho_{new} = \frac{\rho_{predi} h_{predi} A_{cell} + \sum_{b=1}^{nb} (\rho_b q_b \Delta t)}{h_{new} A_{cell}}, \quad (31)$$

8 where h_{new} and ρ_{new} are the updated flow depth and density, respectively; q_b and ρ_b are the
9 discharge and density of the exchange flow across a boundary, respectively; nb is the number
10 of flow boundaries of the cell (i.e. eight); A_{cell} is the area of the cell. By considering the
11 changes of flow and density due to the flow between any two cells, the influence of the spatial
12 differences of hv and $C_v hv$ that are not considered in step 1 is considered in this step.

13 (5) To make the solution more robust, the average values of v^n and v_{predi} are computed and
14 steps (1)-(4) are repeated until the value of v_{predi} converges. Once this is achieved, the values
15 of v_{predi} , h_{new} and ρ_{new} are assigned to v^{n+1} , h^{n+1} and ρ^{n+1} , respectively, and the time step moves
16 forward.

17 2.6 Time stepping and numerical stability

18 On one hand, the time step should be sufficiently small to ensure the numerical stability. On
19 the other hand, the time step should be large enough to attain reasonable computational
20 efficiency. An adaptive time stepping scheme is adopted in this research to ensure both the
21 numerical stability and the computational efficiency, especially for cases which involve a

1 large number of cells so that the simulation time is likely long. The algorithm for the adaptive
2 time stepping scheme is shown in Fig. 6.

3 Three convergence criteria are adopted in this study. The first criterion is the Courant-
4 Friedrich-Lewy (CFL) condition; namely, a particle of fluid should not travel more than the
5 cell size in one time step, Δt . The second criterion states that the percent change of flow depth
6 in one time step should not exceed a specified tolerant value, $TOLP(h)$ (e.g. 10%), which
7 ensures that the flow depth at one cell will not change from a positive value to a negative
8 value within one time step. If the flow moves to a cell with a zero flow depth, the second
9 criterion cannot be satisfied and the third criterion is needed. The third criterion states that the
10 change of flow depth in one time step should not exceed a specified tolerant value, $TOL(h)$
11 (e.g. 0.1 m), which makes the time step move forward even though the second criterion
12 cannot be satisfied. The values of $TOLP(h)$ and $TOL(h)$ depend on required accuracy and the
13 maximum flow depth. Larger values of $TOLP(h)$ and $TOL(h)$ lead to higher computation
14 efficiency but lower accuracy. Hence, if the first criterion and either one of the last two
15 criteria are satisfied for all cells, the time step can move forward successfully, and the time
16 step can be enlarged. Otherwise, the computation for that time step must be abandoned and
17 the time step should be shortened until the required criteria are satisfied.

18 **3 Model verification**

19 In this section, four numerical tests are conducted to verify the performance of the proposed
20 model. In Test 1, an analytical solution to one-dimensional debris flow is adopted to validate
21 the performance of the model in simulating the movement of a debris flow with constant
22 material properties. In Test 2, a two-dimensional dam-break flow problem is adopted to
23 validate the performance of the model in simulating two-dimensional problems. In Test 3, a
24 flume test is adopted to validate the performance of the model in describing the erosion
25 process and material property changes. In Test 4, another flume test is adopted to validate the
26 performance of the model in describing the movement of a debris flow considering the
27 material property changes due to both erosion and deposition.

28 **3.1 Test 1: analytical solution to one-dimensional debris flow with constant** 29 **properties**

30 The problem described by Liu and Mei (1989) is adopted in this test. The materials are
31 initially retained as a triangular pile by a board and the initial profile is shown in Fig. 7. The

1 materials start moving after the board is removed and cease moving finally due to the
2 presence of yield stress. The final profile for the one-dimensional flow is (Liu and Mei, 1989)

$$3 \quad h^2 = \pm \frac{2\tau_y}{\rho g} x + a^2, \quad (32)$$

4 where a is a coefficient; ρ and μ are 1200 kg/m^3 and $5 \text{ Pa}\cdot\text{s}$, respectively (Liu and Mei, 1989).
5 Given an a value of 0.5 m , τ_y is 475 Pa (Liu and Huang, 2006). The bottom surface is
6 assumed to be smooth and the Manning coefficient is hence 0. The resistance parameter for
7 laminar flow, K , is set to be 2500 after several trial computations. The cell size is set to be 0.1
8 m following Liu and Huang (2006). Since the problem is one-dimensional, there are only two
9 flow directions and two flow boundaries for each cell. The width of the flow boundary equals
10 the cell size. The final profiles from the analytical solution and the numerical solution are
11 compared in Fig. 7. The maximum error is only 1%. The model simulates the movement of
12 the debris flow exceptionally well.

13 **3.2 Test 2: two-dimensional dam-break water flow**

14 A two-dimensional partial dam-breach problem reported by Fennema and Hanif Chaudhry
15 (1987) is adopted. A sketch of the problem is shown in Fig. 8a. The computation domain is a
16 channel 200 m in length and 200 m in width. The depth of the reservoir water is 10 m , and the
17 depth of the tail water is 5 m . The boundary is assumed to be frictionless. The dam is assumed
18 to fail instantaneously and the breach width is 75 m . The computation domain is discretised
19 into a grid with cell dimensions of $2.5 \times 2.5 \text{ m}$. The time step is kept at 0.01 s . The flow
20 resistance slope, S_f , is taken as 0 in this test as the channel is assumed frictionless. The water
21 depth at 7.1 s after the dam breaches is shown in Fig. 8(a), which agrees with the result of
22 Fennema and Hanif Chaudhry (1987). Two points in Fig. 8(a) are selected for investigating
23 the variation of water depth with time. The results from the numerical solution using EDDA
24 and two numerical solutions by Fennema and Hanif Chaudhry (1987) are compared in Fig.
25 8(b), which again agree reasonably well.

26 **3.3 Test 3: flume test considering changes in debris flow properties due to** 27 **erosion**

28 A series of flume experiments conducted by Takahashi et al. (1992) is simulated in this
29 numerical test. The width of the flume was 10 cm . Four experiments with different lengths of

1 erodible bed layer ($L = 1, 2, 3, 4$ m) were conducted. The thickness of the erodible bed layer
2 was 10 cm. The slope of the flume was maintained at 18° . A partition and a sampler were
3 installed at the outlet of the flume in the experiment. The partition and sampler are assumed to
4 have no influence on the flow. Fig. 9 shows the experiment setup for the case of $L = 4$ m. The
5 mean particle size, d_{50} , of the bed material was 1.66 mm, and the C_{v*} value was 0.655. During
6 the test, water was introduced from the upstream end at a constant discharge of $2000 \text{ cm}^3/\text{s}$ to
7 produce a debris flow. The measured values of the volumetric sediment concentration, C_v , at
8 the debris flow front when the debris flow front moved 1, 2, 3 and 4 m were 0.25, 0.40, 0.39,
9 0.40, respectively.

10 In the simulation, the flume is discretized into a grid with cell dimensions of 0.02×0.02 m. No
11 flow is allowed across the flume walls. The soil properties and hydrological parameters used
12 to simulate the debris flow considering the erosion process in this test are summarized in
13 Tables 1 and 2, respectively. Some parameters are adopted from Takahashi et al. (1992);
14 namely, c' , d_{50} , ρ_w , ρ_s , ϕ , ϕ_{bed} , s_b , C_{v*} . The values of α_2 and β_2 for computing the dynamic
15 viscosity are adopted from Bisantino et al. (2010). The mean particle size of the samples in
16 the tests of Bisantino et al. (2010) ranged from 0.6 mm to 0.9 mm, which was close to the
17 value of the materials used in the flume tests by Takahashi et al. (1992). The resistance
18 parameter for laminar flow, K , is determined as 500, which is within the recommended range
19 for erodible sand surfaces (FLO-2D Software Inc., 2009). The Manning coefficient is
20 estimated to be 0.10, which is within the recommended range for open grounds with debris
21 (FLO-2D Software Inc., 2009). The values of C_s and K_e are determined based on several trial
22 calculations. The time step is kept at 0.002 s. The calculated C_v values when the debris flow
23 front moves 1, 2, 3 and 4 m are 0.23, 0.39, 0.46, 0.46, respectively. The errors when
24 compared with the measured values are 8%, 2.5%, 17.9%, and 15%, respectively. The model
25 reproduces the erosion process reasonably well.

26 Sensitivity analysis is conducted to investigate the influence of K_e on the erosion process. The
27 results are summarized in Table 3. Four values of K_e are adopted; namely, 1×10^{-5} , 3.5×10^{-5} ,
28 7.5×10^{-5} , $3.5 \times 10^{-4} \text{ m}^3/(\text{Ns})$. The calculated C_v values when the debris flow front moves 1, 2, 3
29 and 4 m are recorded. With the increase of K_e , the erosion process becomes more intensive.
30 For example, C_v reaches 0.46 when the flow marches by only 1 m if K_e is $3.5 \times 10^{-4} \text{ m}^3/(\text{Ns})$;
31 while C_v is only 0.16 when the flow marches by 4 m if K_e is $1 \times 10^{-5} \text{ m}^3/(\text{Ns})$.

3.4 Test 4: flume test considering changes in debris flow properties due to erosion and deposition

Another series of flume tests conducted by Takahashi et al. (1992) is simulated in Test 4. The experiment setup is shown in Fig. 10. In the test series, the flume width was also 10 cm. The bed layer had a length of 3.0 m and a thickness of 10 cm, which was located 5.5 m from the outlet of the flume. A partition with a height of 10 cm was used to retain the sediment in the experiment, and the partition is assumed to have no influence on the flow. A board inclined at 5° longitudinally (Fig. 10b) was connected to the outlet to observe the temporal variations of the shape and elevations of the debris fan. The mean particle size, d_{50} , of the bed material was 3.08 mm, and the C_{v*} value was 0.65. The surface of the bed was glued with the same material to increase the roughness. Water was later introduced from the upstream end at a constant discharge of $600 \text{ cm}^3/\text{s}$ for 20 s to produce a debris flow. To consider the uncertainties of the sample properties, the tests were conducted six times repeatedly. In each run, the discharge at the outlet of the flume was measured. The first two runs are treated as trial runs in this study, and the results of the last four runs are adopted for comparison.

In the simulation, the flume is discretized into a grid with cell dimensions of 0.02×0.02 m. No flow is allowed across the flume walls. Adaptive time steps are adopted in this test following the algorithm in Fig. 6, with a minimum time step of 0.0001 s, a maximum converging time step of 0.001 s, Δt_I of 0.0001 s, Δt_D of 0.0001 s, $TOLP(h)$ of 20%, and $TOL(h)$ of 5 cm. The soil properties and hydrological parameters used to simulate the erosion and deposition processes are summarized in Table 1 and Table 2, respectively, which are obtained following the same methods in Test 3. The value of β_I for computing the yield stress is adopted from Bisantino et al. (2010). The value of α_I is back calculated following the method proposed by Chen et al. (2013). Takahashi et al. (1992) found that the erosion rate was inversely proportional to the mean particle size. Since the mean particle size in Test 4 was nearly twice of that in Test 3, the coefficient of erodibility, K_e , is therefore taken as one half of that in Test 3. The Manning coefficient is determined as 0.1 for the flume covered by the saturated sand and 0.05 for the other parts, which are within the recommended range for open grounds without debris (FLO-2D Software Inc., 2009). The coefficient of deposition rate, δ_d , is determined as 0.03 after trial calculations.

The computed discharges at the outlet and the measured results from the last four experiments are compared in Fig. 11. Time $t = 0$ in Fig. 11 denotes the time when the debris flow front

1 reaches the outlet. As shown in Fig. 11, the model describes very well the movement of the
2 debris flow in the confined channel.

3 When the debris flow moves to the flood board (Fig. 10), it decelerates and deposits gradually.
4 The flow depth, deposit thickness, volumetric sediment concentration, and flow velocity can
5 be monitored for all cells. If deposition occurs somewhere, the deposit thickness there will be
6 larger than zero. The thickness of debris fan is the sum of the flow depth and the deposit
7 thickness. The debris fan in the experimental tests and numerical solution are compared in Fig.
8 12, with contours of the thickness of debris fan. At $t = 5$ s after the debris flow runs out of the
9 outlet, the calculated runout distance of the debris fan (55 cm) is slightly smaller than the
10 experimental result (70 cm) while the calculated width of the debris fan (70 cm) is slightly
11 larger than the experimental result (50 cm). At $t = 10$ s after the debris flow runs out, the
12 calculated runout distance of the debris fan (75 cm) is slightly smaller than the experimental
13 result (85 cm). The calculated width of the debris fan (85 cm) is slightly larger than the
14 experimental result (65 cm). At the final stage, the calculated runout distance (102 cm) is
15 slightly larger than the experimental result (100 cm); and the calculated width of the debris
16 fan (85 cm) is slightly larger than the experimental result (80 cm). The calculated debris
17 thickness distributions at the three moments also match the respective experimental results
18 reasonably well. Hence, the model also describes well the movement of debris flows in the
19 unconfined flat area.

20 Sensitivity analysis is conducted to investigate the influence of deposition rate on the runout
21 characteristics of debris flows. The debris fans at the final stage considering different δ_d
22 values are shown in Fig. 13. The numerical constant, δ_d , of the deposition rate (Eq. 26)
23 governs the deposition speed. With the increase of δ_d , the runout distance decreases while the
24 maximum thickness of the debris fan increases significantly, and most solid materials deposit
25 near the outlet. When the debris flow runs out of the outlet, it decelerates gradually and
26 deposition occurs. Larger δ_d values lead to faster deposition near the outlet. With the
27 deposition process, the amount of the moving debris flow mixture decreases, leading to
28 decreases in the kinematic energy and potential energy, and hence the runout distance of the
29 moving debris flow. Hence, the deposition process influences the runout characteristics of the
30 debris flow significantly.

1 **4 Field application**

2 **4.1 Xiaojiagou debris flow event on 14 August 2010**

3 Rainfall-induced landslides are one of the most catastrophic hazards in mountainous areas
4 (e.g. Chen et al., 2012; Chen et al., 2014b; Raia et al., 2014; Zhang et al., 2013; Zhang et al.,
5 2014). Decisions for effective risk mitigation require hydrological and landslide analyses at
6 the regional scale (e.g. O'Brien et al., 1993; Formetta et al., 2011; Archfield et al., 2013; Chen
7 et al., 2013). The 2008 Wenchuan earthquake triggered numerous landslides, leaving a large
8 amount of loose materials on the hill slopes or channels. From 12 August 2010 to 14 August
9 2010, a storm swept the epicentre, Yingxiu, and its vicinity, triggering a catastrophic debris
10 flow in Xiaojiagou Ravine (Fig. 14). About $1.01 \times 10^6 \text{ m}^3$ of deposit was brought out in the
11 form of a channelized debris flow. According to the rainfall record at Yingxiu that is 5 km
12 from Xiaojiagou Ravine, the total rainfall amount was 220 mm in a period of 40 h (Chen et al.,
13 2012). The debris flow was witnessed to occur at the ravine mouth at about 5:00 am on 14
14 August (i.e. 36 h after the storm started) and lasted about 30 minutes. The cumulative rainfall
15 from the beginning of the storm to the occurrence of the debris flow was 188 mm. The runout
16 materials of the debris flow buried 1100 m of road, blocked the Yuzixi River, formed a debris
17 flow barrier lake and raised the river bed by at least 15 m.

18 Interpretation of the satellite images taken before and after the debris flow reveals that the
19 source material of this debris flow was mainly the channel colluvium (Chen et al., 2012). The
20 deposits in the main channel marked 'location of the main source material' in Figs. 14 and 15
21 had a volume of approximately $0.74 \times 10^6 \text{ m}^3$ before the debris flow event and much of it had
22 been washed away (Chen et al., 2012). Based on interpretation of satellite images and field
23 investigations, the observed deposition zone is determined and shown in Fig. 14.

24 **4.2 Determination of input information**

25 The study area is divided into two domains, one for rainfall-runoff simulation and the other
26 for debris flow runout simulation (Fig. 15). Grid systems are created within the two domains
27 with grid sizes of $30 \times 30 \text{ m}$ for domain one and $15 \times 15 \text{ m}$ for domain two. After the
28 Xiaojiagou debris flow, detailed field investigations and laboratory tests were conducted. The
29 hydrological parameters for rainfall runoff simulation and debris flow runout simulation have
30 been proposed by Chen et al. (2013) and are summarized in Table 4.

1 Rainfall runoff simulation is conducted first in domain one using FLO-2D (FLO-2D Software
 2 Inc., 2009). The rainfall data at Yingxiu is adopted. The runoff water would be retained by the
 3 colluvium and accumulate behind the landslide deposits, forming landslide barrier ponds. The
 4 cumulative runoff water at Section 1-1 (Figs. 14 and 15) can be computed, which is applied at
 5 Section 1-1 as the inflow hydrograph for debris flow runout simulation in domain two. Debris
 6 flow would occur when the barrier ponds breach. The source materials are assumed to be
 7 saturated before the occurrence of the debris flow. As water flows over the source material,
 8 erosion occurs if the conditions in Eqs. (18)-(21) are met. Since the debris flow was witnessed
 9 to occur at the ravine mouth about 36 h after the storm started and lasted about 30 minutes,
 10 the cumulative runoff water at Section 1-1 in Fig. 14 at 36 h after the storm started is adopted
 11 to create the inflow hydrograph, and the surface runoff is determined to be $0.5 \times 10^6 \text{ m}^3$. The
 12 observed outflow hydrographs for landslide dams in the Wenchuan earthquake zone (e.g.
 13 Tangjiashan and Xiaogangjian) show a peak during the dam collapse process (Chang and
 14 Zhang, 2010). The two landslide dams breached due to overtopping erosion. Therefore, the
 15 inflow hydrograph for the Xiaojiagou debris flow is assumed to be an isosceles triangle for
 16 simplicity (Fig. 16). The duration and the peak discharge are 0.5 h and $556 \text{ m}^3/\text{s}$, respectively.
 17 The area of the inflow hydrograph is equal to $0.5 \times 10^6 \text{ m}^3$.

18 In domain two, the source material is distributed into 329 cells with a thickness of 10 m. The
 19 internal friction angle, ϕ_{bed} , for the source material is determined as 37° according to the test
 20 results of Zhao et al. (2013). Since the source material has a very low content of silt and clay
 21 ($< 2\%$) according to sieving tests (Chen et al., 2012), the effective cohesion, c' , is assumed to
 22 be 0 in the debris flow runout simulation. The values of d_{50} , ρ_s , C_{v*} are determined based on
 23 field and laboratory tests. The method and testing results have been reported in detail by Chen
 24 et al. (2012). Since the source material is assumed to be saturated, s_b is 1. K_e is determined
 25 using an empirical equation developed based on field tests in the Wenchuan earthquake zone
 26 by Chang et al. (2011):

$$27 \quad K_e = 0.020075e^{4.77} C_u^{-0.76}, \quad (33)$$

28 where e is the void ratio and C_u is the coefficient of uniformity. The values of e and C_u are
 29 0.54 and 39, respectively, based on the sieving tests. Hence, K_e is $6.6 \times 10^{-5} \text{ m}^3/(\text{Ns})$. The soil
 30 properties are summarized in Table 1. The values of α_1 , β_1 , α_2 , β_2 , K , and n are determined
 31 following Chen et al. (2013). The value of C_s and δ_d are determined after several trial

1 computations. The hydrological parameters for simulating the erosion and deposition
2 processes are summarized in Table 2. Adaptive time steps are adopted in this test following
3 the algorithm in Fig. 6, with a minimum time step of 0.01 s, a maximum converging time step
4 of 1.0 s, Δt_I of 0.01 s, Δt_D of 0.02 s, $TOLP(h)$ of 20%, and $TOL(h)$ of 0.5 m.

5 **4.3 Changes in debris flow properties during the flow process**

6 The values of the volumetric sediment concentration, C_v , when the debris flow reaches
7 Sections 2-2, 3-3, 4-4 in Fig. 14 are computed, which are 0.13, 0.23, 0.49, respectively. With
8 the increase of C_v , the yield stress and dynamic viscosity also increase significantly as Fig. 3
9 shows.

10 The change of C_v with time at Section 3-3 is shown in Fig. 17. C_v is 0.23 at $T = 0$ when the
11 forefront reaches the section, which can be viewed as the precursory surge in Fig. 1.
12 Afterwards, C_v increases very quickly to a peak value of about 0.5, which can be viewed as
13 the boulder front in Fig. 1. After the boulder front passes, C_v sustains at the peak value for
14 some time (about 60 s), which can be viewed as the fully developed debris flow in Fig. 1.
15 After that, C_v decreases gradually to a lower level, which can be viewed as the hyper-
16 concentrated flow in Fig. 1. This flow region is erosive and the bedding solid materials can be
17 entrained. The erosion process upstream Section 3-3 lasts about 300 s.

18 **4.4 Comparison between simulated and observed results**

19 The volume of the simulated debris flow is about $1.0 \times 10^6 \text{ m}^3$. Since the sum of the inflow
20 water ($0.5 \times 10^6 \text{ m}^3$) and the saturated source material ($0.74 \times 10^6 \text{ m}^3$) is $1.24 \times 10^6 \text{ m}^3$,
21 approximately $0.24 \times 10^6 \text{ m}^3$ of the source material is not entrained into the debris flow in the
22 simulation. Hence, not all the source material erodes.

23 The simulated and observed deposition zones are shown in Fig. 18a. The simulated inundated
24 area and runout distance match the observed results reasonably well. It is noted that the debris
25 fan front has very small depths; the fan front is the precursory surge in front of the boulder
26 front in Fig. 1. The distribution of the maximum flow velocity is shown in Fig. 18b, which
27 indicates that the debris flow moves very rapidly, especially in the ravine channel. Taking into
28 account the large volume, the debris flow is very destructive, which has been observed by
29 Chen et al. (2012).

1 The comparison between the simulation results and the observations suggests that the model
2 evaluates well the debris flow volume considering the erosion process. The inundated area
3 and the runout distance can also be predicted reasonably well.

4 **5 Limitations of EDDA**

5 The mathematical model proposed in this study has limitations due to the simplifying
6 assumptions and approximations in the underlying theory. The main limitations are as follows:

7 (1) The model is suitable for describing the initiation and movement of debris flows
8 originated from runoff-driven channel bed failure or breaching of landslide dams by
9 overtopping erosion, which has been tested in this study. The model is also able to consider
10 surficial material entrainment from collapses of bank material or detached landslide material
11 as shown in the governing differential equations. But the latter capability has not been tested
12 and further work is needed.

13 (2) The new model is suitable for channels and flat alluvial fans, but may not be ideal for
14 steep terrains.

15 (3) The flow velocity in each of the eight flow directions is computed independently
16 without considering the flow velocity gradient in the orthogonal direction (Eqs. 3 and 4). Such
17 influence is not significant in a confined channel since the orthogonal gradient is small. In an
18 unconfined flat area, the eight flow directions account for the influence to certain extent, but
19 further work is needed to test the performance of the model.

20 (4) Further work is needed to test the performance of some empirical equations adopted in
21 the model.

22 (5) The governing equations are in a depth-integrated form, hence the particle segregation
23 in the vertical direction cannot be considered.

24 (6) A hydrostatic pressure distribution is assumed along the vertical direction, which
25 affects the computed yield stress.

26 (7) The suspension coefficient, C_s , can vary with mean particle size and discharge. In

1 Tests 3 and 4, C_s is assumed to be a constant for simplicity. Further work is desired to
2 properly determine this parameter.

3 **6 Summary and conclusions**

4 A new depth-integrated numerical model for simulating debris flow erosion, deposition, and
5 property changes (EDDA) is developed in this study. The model considers the changes in
6 debris flow density, yield stress, and dynamic viscosity, as well as the influences of such
7 changes on the runout characteristics of the debris flow.

8 The model is unique in that it considers erosion and deposition processes, and changes in
9 debris flow mass, debris flow properties and topography due to erosion and deposition.
10 Considering the partly suspended solid particles at limit equilibrium, the yield stress of the
11 debris flow mixture estimated using the Mohr-Coulomb equation is suitable for water flows,
12 hyper-concentrated flows, and fully developed debris flows. An adaptive time stepping
13 algorithm is developed to assure both numerical stability and computational efficiency.

14 Four numerical tests have been conducted to verify the performance of the model. In Test 1,
15 an analytical solution to one-dimensional debris flow with constant properties is adopted.
16 Comparison between the numerical solution and the analytical solution indicates that the
17 model simulates exceptionally well the one-dimensional movement of debris flow with
18 constant properties. In Test 2, a two-dimensional dam-break water flow problem is adopted.
19 The model simulates very well the two-dimensional dam-break water flow. Flume tests are
20 simulated in Tests 3 and 4. The calculated volumetric sediment concentration at the debris
21 flow front agrees with the experimental results reasonably well in Test 3. In Test 4, the model
22 simulates reasonably well the erosion and deposition processes, and the movement of the
23 multi-direction debris flows in the confined channel and the unconfined flat area in terms of
24 the discharge hydrographs at the outlet and the time-varying geometry and elevations of the
25 debris fan. Sensitivity analyses in Tests 3 and 4 indicate that erosion and deposition processes
26 influence the property changes and runout characteristics significantly.

27 The model is also applied to simulate a large-scale debris flow in Xiaojiagou Ravine to test
28 the performance of the model in catchment-scale simulations. The model well describes the
29 changes in debris flow properties and estimates the volume of debris flow. Considering the
30 deposition process, the inundated area and the runout distance are predicted properly. The

1 model is shown to be a powerful tool for debris flow risk assessment in a large area and
2 intended for use as a module in a real-time warning system for debris flows.

3

4 **Code availability**

5 EDDA is written in FORTRAN, which can be compiled by Intel FORTRAN Compilers. The
6 source code is enclosed as supplement files. The main subroutine is dfs.F90, which contains
7 the numerical solution algorithm for solving the governing equations. Two input files are
8 needed. One is edda_in.txt, which is the file for inputting material properties and hydrological
9 parameters, and setting controlling options. EDDA is designed as the debris-flow simulation
10 part of a cell-based model for analysing regional slope failures and debris flows, so the
11 edda_in.txt file also includes the material properties and controlling options for slope stability
12 analysis. The other is inflow.txt, which is the inflow hydrograph file. Digital terrain data (e.g.
13 surface elevation, slope gradient, erodible layer thickness) are included in separate ASCII grid
14 files and enclosed in the data folder. Output files are stored in the result folder. Investigated
15 variables at selected points are stored in EDDALog.txt.

16

17 **Acknowledgements**

18 This research was substantially supported by Sichuan Department of Transportation and
19 Communications, the Natural Science Foundation of China (Grant No. 51129902), and the
20 Research Grants Council of the Hong Kong SAR (No. 16212514).

21

22 **References**

23 Alexandrov, Y., Laronne, J. B., and Reid, I.: Suspended sediment concentration and its
24 variation with water discharge in a dryland ephemeral channel, northern Negev, Israel,
25 *Journal of Arid Environments*, 53(1), 73-84, 2003.

26 Akan, A. O., and Yen, B. C.: Diffusion-wave flood routing in channel networks, *Journal of*
27 *the Hydraulics Division*, 107(6), 719-732, 1981.

28 Archfield, S. A., Steeves, P. A., Guthrie, J. D., and Ries III K. G.: Towards a publicly
29 available, map-based regional software tool to estimate unregulated daily streamflow at
30 ungauged rivers, *Geoscientific Model Development*, 6, 101-115, 2013.

- 1 Armanini, A., Fraccarollo, L., and Rosatti, G.: Two-dimensional simulation of debris flows in
2 erodible channels, *Computers & Geosciences*, 35(5), 993-1006, 2009.
- 3 Bartelt, P., Buehler, Y., Christen, M., Deubelbeiss, Y., Graf, C., McArdell, B., Salz, M., and
4 Schneider, M.: A numerical model for debris flow in research and practice, User Manual v1.5
5 Debris Flow, WSL Institute for Snow and Avalanche Research SLF, 2013.
- 6 Beguer á, S., Van Asch, T. W., Malet, J. P., and Gröndahl, S.: (2009). A GIS-based numerical
7 model for simulating the kinematics of mud and debris flows over complex terrain, *Natural
8 Hazards and Earth System Science*, 9, 1897-1909, 2009.
- 9 Berger, C., McArdell, B. W., Fritschi, B., and Schlunegger, F.: A novel method for measuring
10 the timing of bed erosion during debris flows and floods, *Water Resources Research*,
11 46(W02502), doi:10.1029/2009WR007993, 2010.
- 12 Bisantino, T., Fischer, P., and Gentile, F.: Rheological characteristics of debris-flow material
13 in South-Gargano watersheds, *Natural Hazards*, 54(2), 209-223, 2010.
- 14 Boss Corporation: DAMBRK-User's manual. Boss International Inc., Madison, Wisconsin,
15 USA, 1989.
- 16 Cannon, S. H., and Savage, W. Z.: A mass change model for the estimation of debris flow
17 runout, *The Journal of Geology*, 96, 221-227, 1988.
- 18 Chang, D. S., and Zhang, L. M.: Simulation of the erosion process of landslide dams due to
19 overtopping considering variations in soil erodibility along depth, *Natural Hazards and Earth
20 System Sciences*, 10, 933-946, 2010.
- 21 Chang, D. S., Zhang, L. M., Xu, Y., and Huang, R. Q.: Field testing of erodibility of two
22 landslide dams triggered by the 12 May Wenchuan earthquake, *Landslides*, 8(3), 321-332,
23 2011.
- 24 Chen, H., Crosta, G. B., and Lee, C. F.: Erosional effects on runout of fast landslides, debris
25 flows and avalanches: a numerical investigation, *Geotechnique*, 56(5), 305-322, 2006.
- 26 Chen, H. X., Zhang, L. M., Chang, D. S., and Zhang, S.: Mechanisms and runout
27 characteristics of the rainfall-triggered debris flow in Xiaojiagou in Sichuan Province, China,
28 *Natural Hazards*, 62(3), 1037-1057, 2012.

1 Chen, H. X., Zhang, L. M., Zhang, S., Xiang, B., and Wang X. F.: Hybrid simulation of the
2 initiation and runout characteristics of a catastrophic debris flow, *Journal of Mountain*
3 *Science*, 10(2), 219-232, 2013.

4 Chen, H. X., Zhang, L. M., and Zhang, S.: Evolution of debris flow properties and physical
5 interactions in debris-flow mixtures in the Wenchuan earthquake zone, *Engineering Geology*,
6 182, 136-147, 2014a.

7 Chen, H. X., and Zhang, L. M.: A physically-based distributed cell model for predicting
8 regional rainfall-induced shallow slope failures, *Engineering Geology*, 176, 79-92, 2014b.

9 Coussot, P., Laigle, D., Arattano, M., Deganutti, A., and Marchi, L.: Direct determination of
10 rheological characteristics of debris flow, *Journal of Hydraulic Engineering*, 124(8), 865-868,
11 1998.

12 Crosta, G. B., Imposimato, S., and Roddeman, D. G.: Numerical modelling of large landslides
13 stability and runout, *Natural Hazards and Earth System Science*, 3(6), 523-538, 2003.

14 Denlinger, R. P., and Iverson, R. M.: Flow of variably fluidized granular masses across three-
15 dimensional terrain: 2. Numerical predictions and experimental tests, *Journal of Geophysical*
16 *Research: Solid Earth*, 106(B1), 553-566, 2001.

17 Egashira, S., Honda, N., and Itoh, T.: Experimental study on the entrainment of bed material
18 into debris flow, *Physics and Chemistry of the Earth, Part C: Solar, Terrestrial & Planetary*
19 *Science*, 26(9), 645-650, 2001.

20 Fennema, R. J., and Hanif Chaudhry, M.: Simulation of one-dimensional dam-break flows,
21 *Journal of Hydraulic Research*, 25(1), 41-51, 1987.

22 FLO-2D Software Inc.: FLO-2D reference manual, Nutrioso, Arizona, USA, 2009.

23 Formetta, G., Mantilla, R., Franceschi, S., Antonello, A., and Rigon, R.: The JGrass-NewAge
24 system for forecasting and managing the hydrological budgets at the basin scale: models of
25 flow generation and propagation/routing, *Geoscientific Model Development*, 4(4), 943-955,
26 2011.

27 Fraccarollo, L., and Papa, M.: Numerical simulation of real debris-flow events, *Physics and*
28 *Chemistry of the Earth, Part B: Hydrology, Oceans and Atmosphere*, 25, 757-763, 2000.

- 1 Ghilardi, P., Natale, L., and Savi, F.: Modeling debris flow propagation and deposition,
2 Physics and Chemistry of the Earth, Part C: Solar, Terrestrial & Planetary Science, 26(9),
3 651-656, 2001.
- 4 Hanson, G. J.: Surface erodibility of earthen channels at high stresses part I-open channel
5 testing, Transactions of the ASAE, 33(1), 127-131, 1990.
- 6 Hungr, O.: A model for the runout analysis of rapid flow slides, debris flows, and avalanches,
7 Canadian Geotechnical Journal, 32, 610-623, 1995.
- 8 Hungr, O., McDougall, S., and Bovis, M.: Entrainment of material by debris flows. In Debris-
9 flow hazards and related phenomena (eds. M. Jakob and O. Hungr), Springer-Praxis,
10 Chichester, UK, pp 135-158, 2005.
- 11 Hungr, O., and McDougall, S.: Two numerical models for landslide dynamic analysis,
12 Computers & Geosciences, 35(5), 978-992, 2009.
- 13 Iverson, R. M., Reid, M. E., Logan, M., LaHusen, R. G., Godt, J. W., and Griswold, J. P.:
14 Positive feedback and momentum growth during debris-flow entrainment of wet bed sediment,
15 Nature Geoscience, 4(2), 116-121, 2011.
- 16 Iverson, R. M.: Elementary theory of bed-sediment entrainment by debris flows and
17 avalanches, Journal of Geophysical Research: Earth Surface, 117(F03006),
18 doi:10.1029/2011JF002189, 2012.
- 19 Julien, P. Y., and Lan, Y.: Rheology of hyperconcentrations, Journal of Hydraulic
20 Engineering, 117(3), 346-353, 1991.
- 21 Kwan, J. S., and Sun, H. W.: An improved landslide mobility model, Canadian Geotechnical
22 Journal, 43(5), 531-539, 2006.
- 23 Li, W. C., Li, H. J., Dai, F. C., and Lee, L. M.: Discrete element modelling of a rainfall-
24 induced flowslide, Engineering Geology, 149, 22-34, 2012.
- 25 Liu, K. F., and Mei, C. C.: Slow spreading of a sheet of Bingham fluid on an inclined plane,
26 Journal of Fluid Mechanics, 207, 505-529, 1989.
- 27 Liu, K. F., and Huang, M. C.: Numerical simulation of debris flow with application on hazard
28 area mapping, Computational Geosciences, 10(2), 221-240, 2006.

1 Major, J. J., and Pierson, T. C.: Debris flow rheology: experimental analysis of fine-grained
2 slurries, *Water Resources Research*, 28(3), 841-857, 1992.

3 McDougall, S., and Hungr, O.: Dynamic modelling of entrainment in rapid landslides,
4 *Canadian Geotechnical Journal*, 42(5), 1437-1448, 2005.

5 Medina, V., Hürlimann, M., and Bateman, A.: Application of FLATModel, a 2D finite
6 volume code, to debris flows in the northeastern part of the Iberian Peninsula, *Landslides*,
7 5(1), 127-142, 2008.

8 O'Brien, J. S., and Julien, P. Y.: Laboratory analysis of mudflow properties, *Journal of*
9 *Hydraulic Engineering*, 114(8), 877-887, 1988.

10 O'Brien, J. S., Julien, P. Y., and Fullerton, W. T.: Two-dimensional water flood and mudflow
11 simulation, *Journal of Hydraulic Engineering*, 119, 244-261, 1993.

12 Ouyang, C., He, S., and Tang, C.: Numerical analysis of dynamics of debris flow over
13 erodible beds in Wenchuan earthquake-induced area, *Engineering Geology*,
14 <http://dx.doi.org/10.1016/j.enggeo.2014.07.012>, 2014.

15 Pastor, M., Haddad, B., Sorbino, G., Cuomo, S., and Drempetic, V.: A depth-integrated,
16 coupled SPH model for flow-like landslides and related phenomena, *International Journal for*
17 *Numerical and Analytical Methods in Geomechanics*, 33(2), 143-172, 2009.

18 Pierson, T. C., and Scott, K. M.: Downstream dilution of a lahar: transition from debris flow
19 to hyperconcentrated streamflow, *Water Resources Research*, 21(10), 1511-1524, 1985.

20 Quan Luna, B., Remaître, A., van Asch, T. W., Malet, J. P., and Van Westen, C. J.: Analysis
21 of debris flow behavior with a one dimensional run-out model incorporating entrainment,
22 *Engineering geology*, 128, 63-75, 2012.

23 Raia, S., Alvioli, M., Rossi, M., Baum, R. L., Godt, J. W., and Guzzetti, F.: Improving
24 predictive power of physically based rainfall-induced shallow landslide models: a
25 probabilistic approach, *Geoscientific Model Development*, 7, 495-514, 2014.

26 Rickenmann, D.: Hyperconcentrated flow and sediment transport at steep slopes, *Journal of*
27 *Hydraulic Engineering*, 117(11), 1419-1439, 1991.

28 Schatzmann, M., Bezzola, G. R., Minor, H. E., Windhab, E. J., and Fischer, P.: Rheometry for
29 large-particulated fluids: analysis of the ball measuring system and comparison to debris flow
30 rheometry, *Rheologica Acta*, 48(7), 715-733, 2009.

1 Sosio, R., and Crosta, G. B.: Rheology of concentrated granular suspensions and possible
2 implications for debris flow modelling, *Water Resources Research*, 45(W03412),
3 doi:10.1029/2008WR006920, 2009.

4 Takahashi, T., Nakagawa, H., Harada, T., and Yamashiki, Y.: Routing debris flows with
5 particle segregation, *Journal of Hydraulic Engineering*, 118(11), 1490-1507, 1992.

6 Takahashi, T.: *Debris flow: mechanics, prediction and countermeasures*, Taylor & Francis,
7 2007.

8 van Asch, Th. W. J., Tang, C., Alkema, C., Zhu, J., and Zhou, W.: An integrated model to
9 assess critical rainfall thresholds for run-out distances of debris flows, *Natural Hazards*, 70,
10 299-311, 2014.

11 Voellmy, A.: Uber die Zerstorkraft von Lawinen. *Schweizerische Bauzeitung*, 73, 212-
12 285, 1955.

13 Zhao, H. F., Zhang, L. M., and Chang, D. S.: Behaviour of coarse widely graded soils under
14 low confining pressures, *Journal of Geotechnical and Geoenvironmental Engineering*, ASCE,
15 139, 35-48, 2013.

16 Zhang, S., Zhang, L. M., and Chen, H. X.: Relationships among three repeated large-scale
17 debris flows at the Pubugou Ravine in the Wenchuan earthquake zone, *Canadian*
18 *Geotechnical Journal*, 51(9), 951-965, 2014.

19 Zhang, S., Zhang, L. M., Chen, H. X., Yuan, Q., and Pan, H.: Changes in runout distances of
20 debris flows over time in the Wenchuan Earthquake zone, *Journal of Mountain Sciences*,
21 10(2), 281-292, 2013.

22

Table 1. Soil Properties in Test 3, Test 4 and Field Application.

Test No.	c' (kPa)	d_{50} (mm)	ρ_w (kg/m ³)	ρ_s (kg/m ³)	ϕ (°)	ϕ_{bed} (°)	s_b	C_v^*	K_e [m ³ /(Ns)]
Test 3	0	1.66	1000	2650	37	37	1	0.655	7×10^{-5}
Test 4	0	3.08	1000	2650	35	35	1	0.650	3.5×10^{-5}
Field application	0	35	1000	2750	37	37	1	0.65	6.6×10^{-5}

Table 2. Hydrological Parameters for Simulating the Erosion and Deposition Processes in Test 3, Test 4 and Field Application.

Test No.	C_s	α_1 (kPa)	β_1	α_2 (Pa.s)	β_2	K	n	δ_d
Test 3	0.4	NA	NA	0.02	2.97	500	0.1	NA
Test 4	0.4	0.016	3.51	0.02	2.97	500	0.05 & 0.1	0.03
Field application	0.5	3.8	3.51	0.02	2.97	2500	0.16	0.02

Table 3. Results of Erosion Sensitivity Analysis in Test 3.

K_e [m ³ /(Ns)]	C_v			
	1 m	2 m	3 m	4 m
1×10^{-5}	0.04	0.1	0.12	0.16
3.5×10^{-5}	0.13	0.24	0.32	0.39
7×10^{-5}	0.23	0.39	0.46	0.46
3.5×10^{-4}	0.46	0.46	0.46	0.46

Table 4. Hydrological Parameters for Rainfall-Runoff and Debris Flow Runout Simulations in Field Application.

Simulation type	Manning coefficient	Initial saturation	Final saturation	Soil porosity	Initial abstraction (mm)	Saturated hydraulic conductivity (mm/h)	Soil suction head (mm)
Rainfall runoff	0.3	0.33	1.0	0.35	6	3.6	51
Debris flow	0.16	1.0	1.0	0.35	0	NA	NA

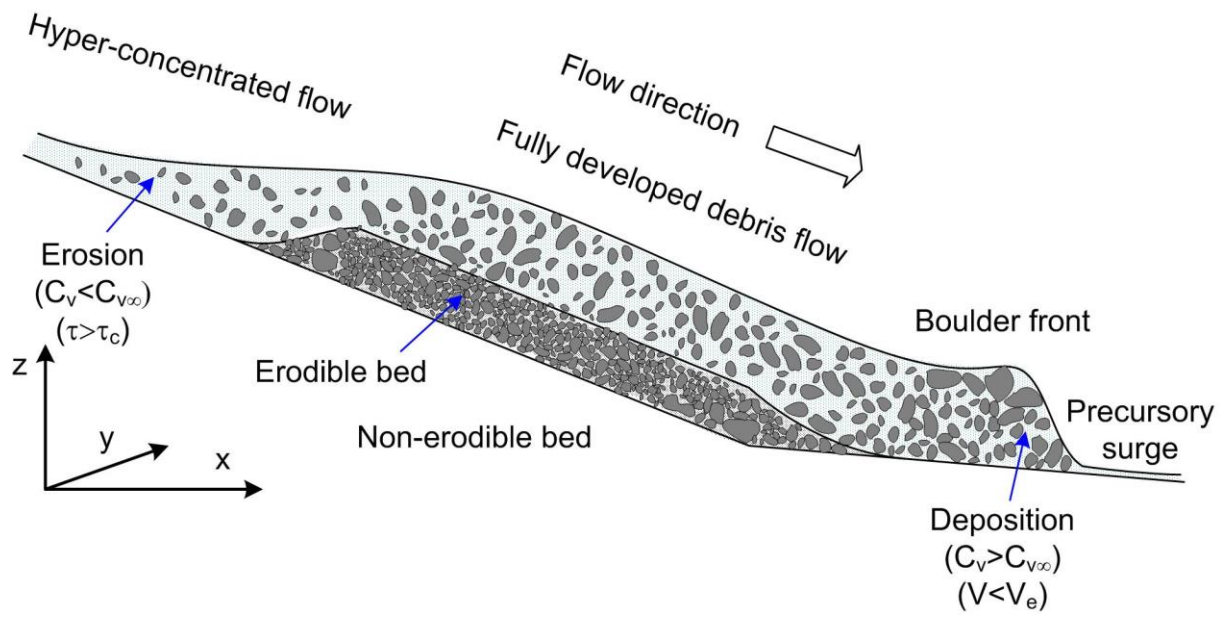


Figure 1. Erosion, deposition and property changes in debris flow.

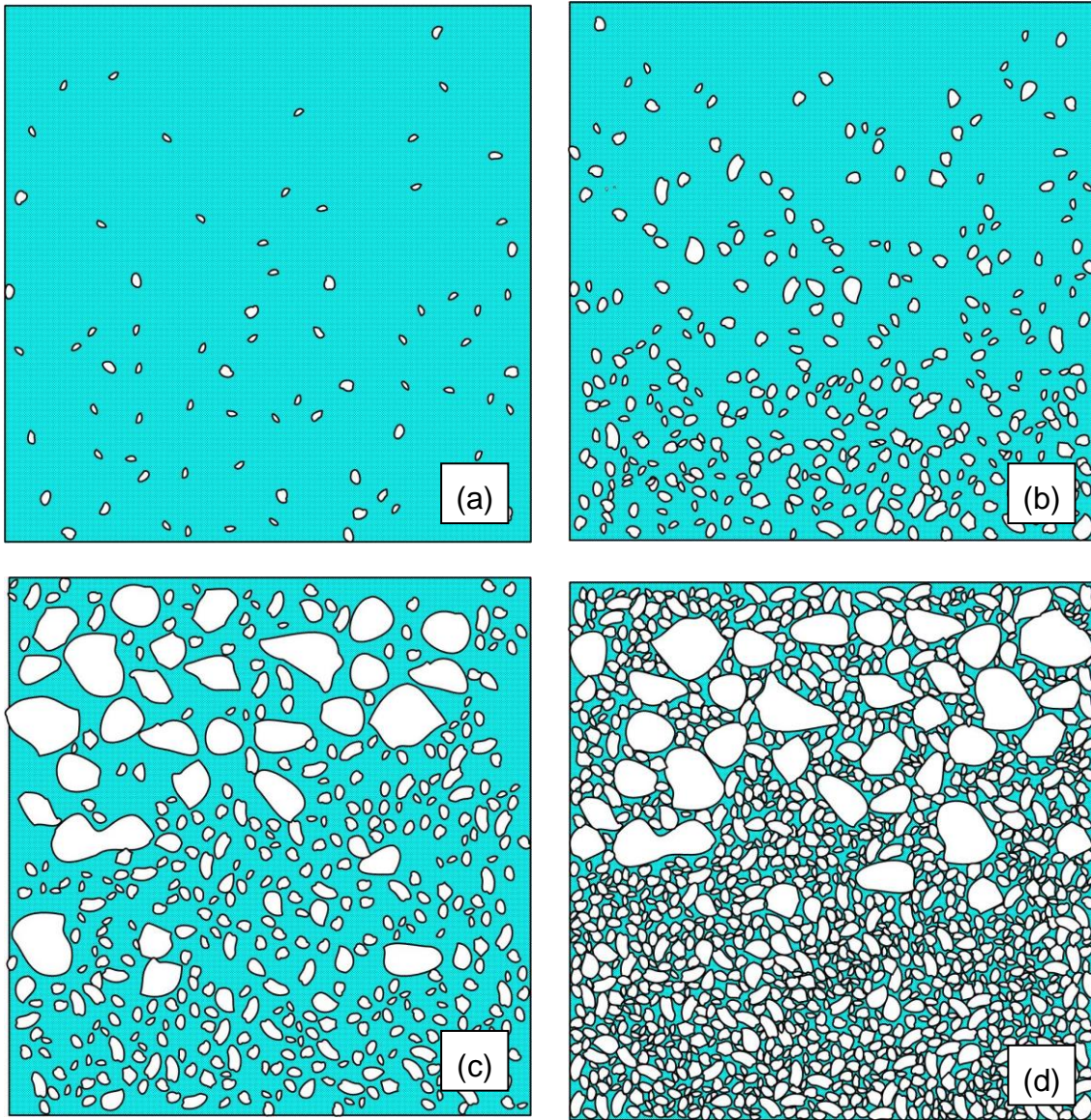


Figure 2. Changes of volumetric sediment concentration of debris flow: (a) clear water flow; (b) hyper-concentrated flow; (c) fully developed debris flow; (d) deposit.

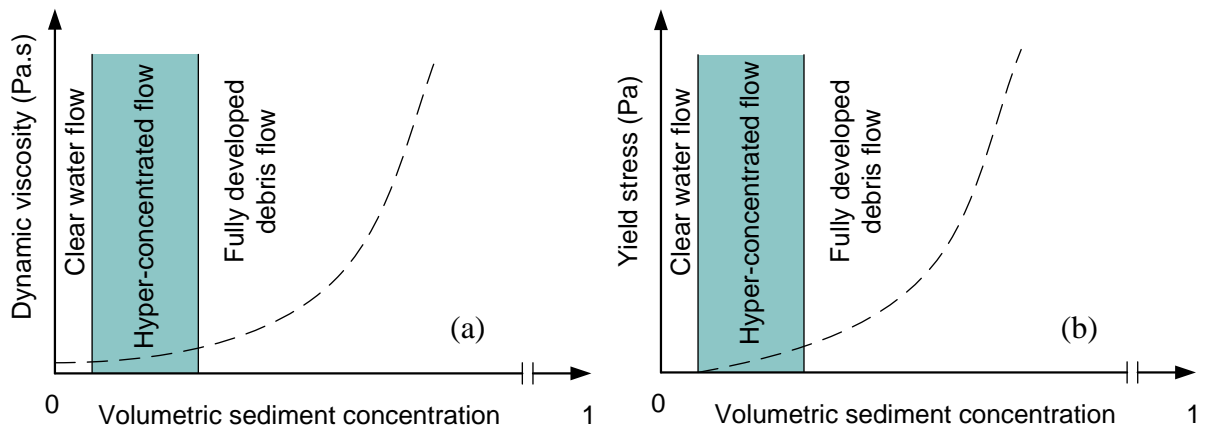


Figure 3. Changes in dynamic viscosity and yield stress with volumetric sediment concentration: (a) dynamic viscosity; (b) yield stress.

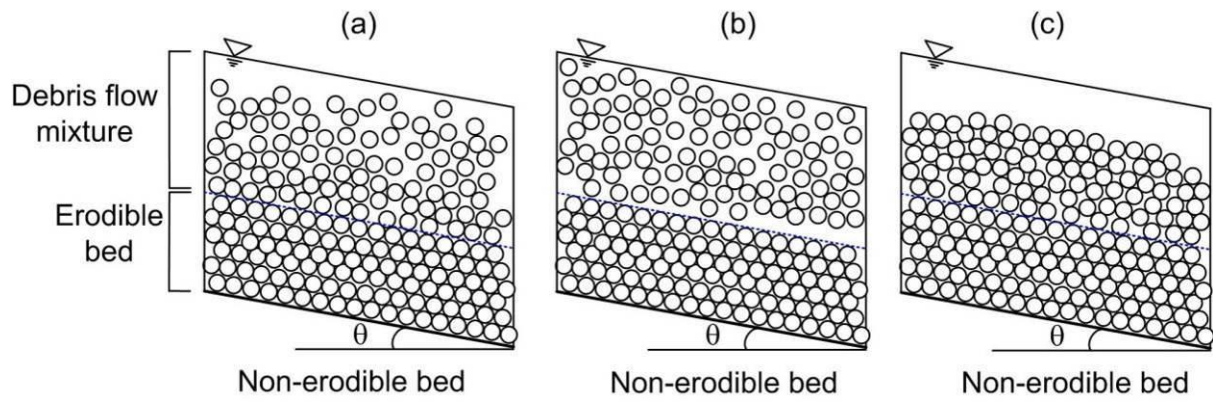


Figure 4. Three typical suspension scenarios: (a) partial suspension, $0 < C_s < 1$; (b) full suspension, $C_s = 1$; (c) no suspension, $C_s = 0$.

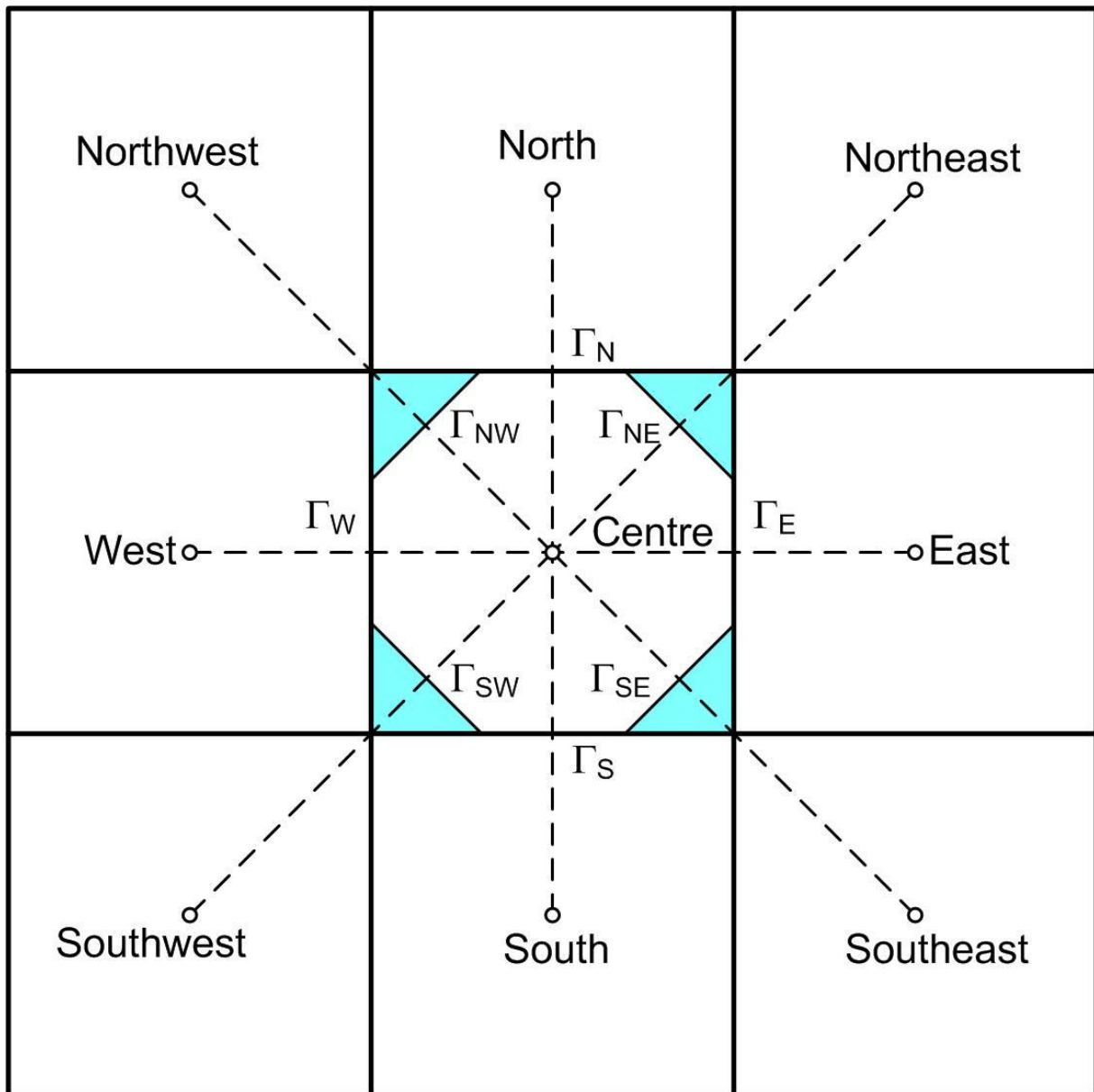


Figure 5. Eight flow directions and flow boundaries of each cell.

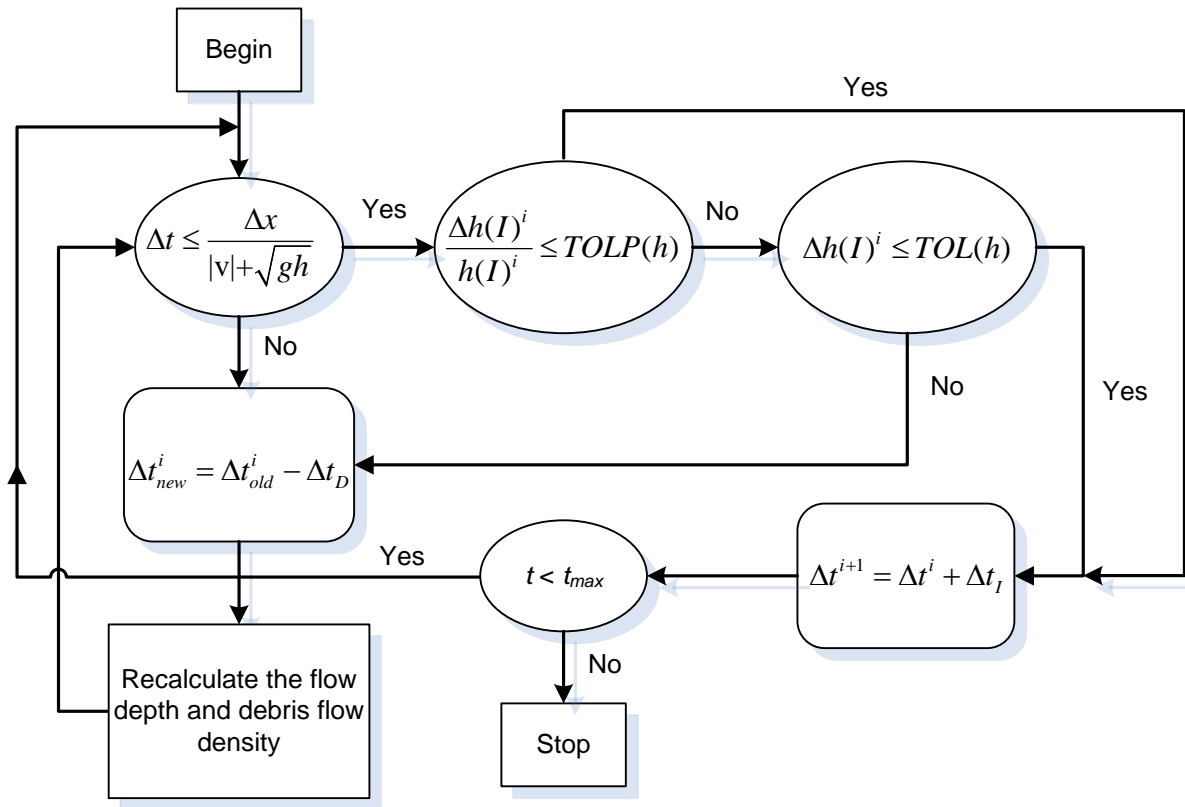


Figure 6. Algorithm for adaptive time stepping. I : cell I ; $\Delta h(I)^i$: change of flow depth of cell I during time step i ; $h(I)^i$: flow depth of cell I during time step i ; $TOLP(h)$: tolerable value of percent change of flow depth during a time step; $TOL(h)$: tolerable value of change of flow depth during a time step; Δt_I : increment of time step; Δt_D : decrement of time step.

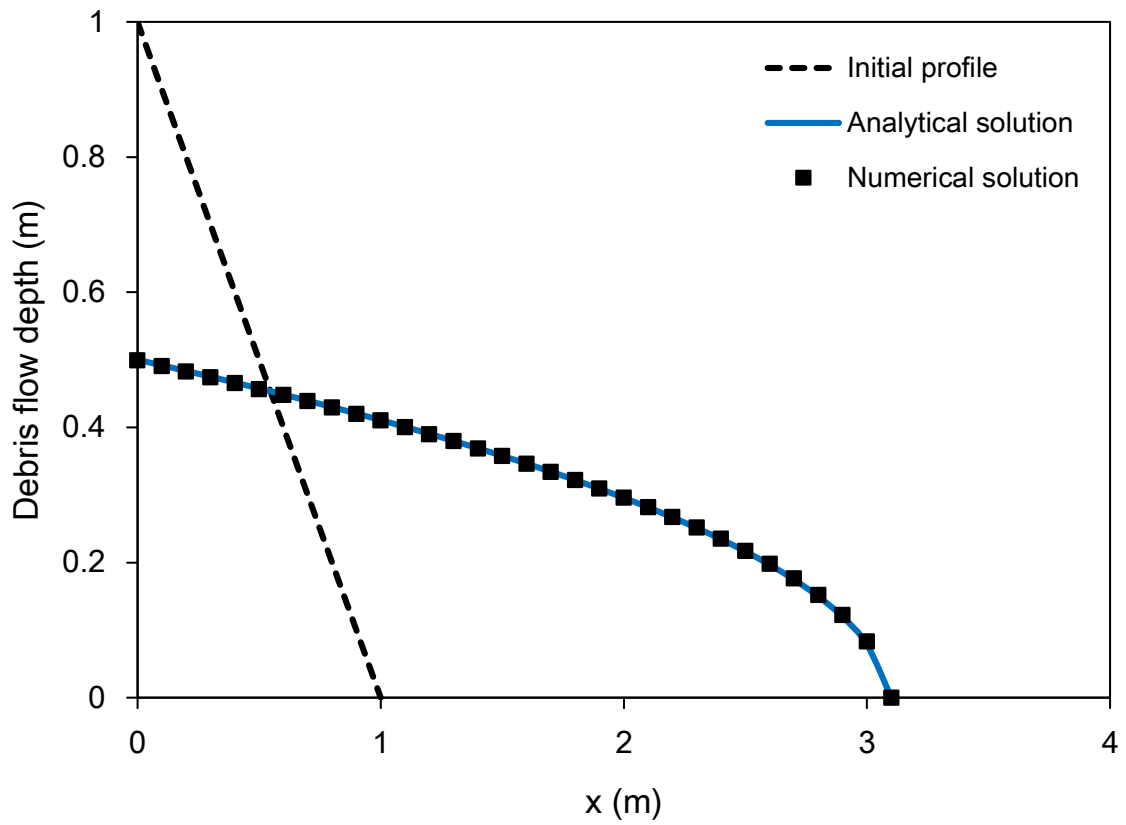


Figure 7. Comparison of the final debris flow depth profiles from the analytical solution and the numerical solution in Test 1.

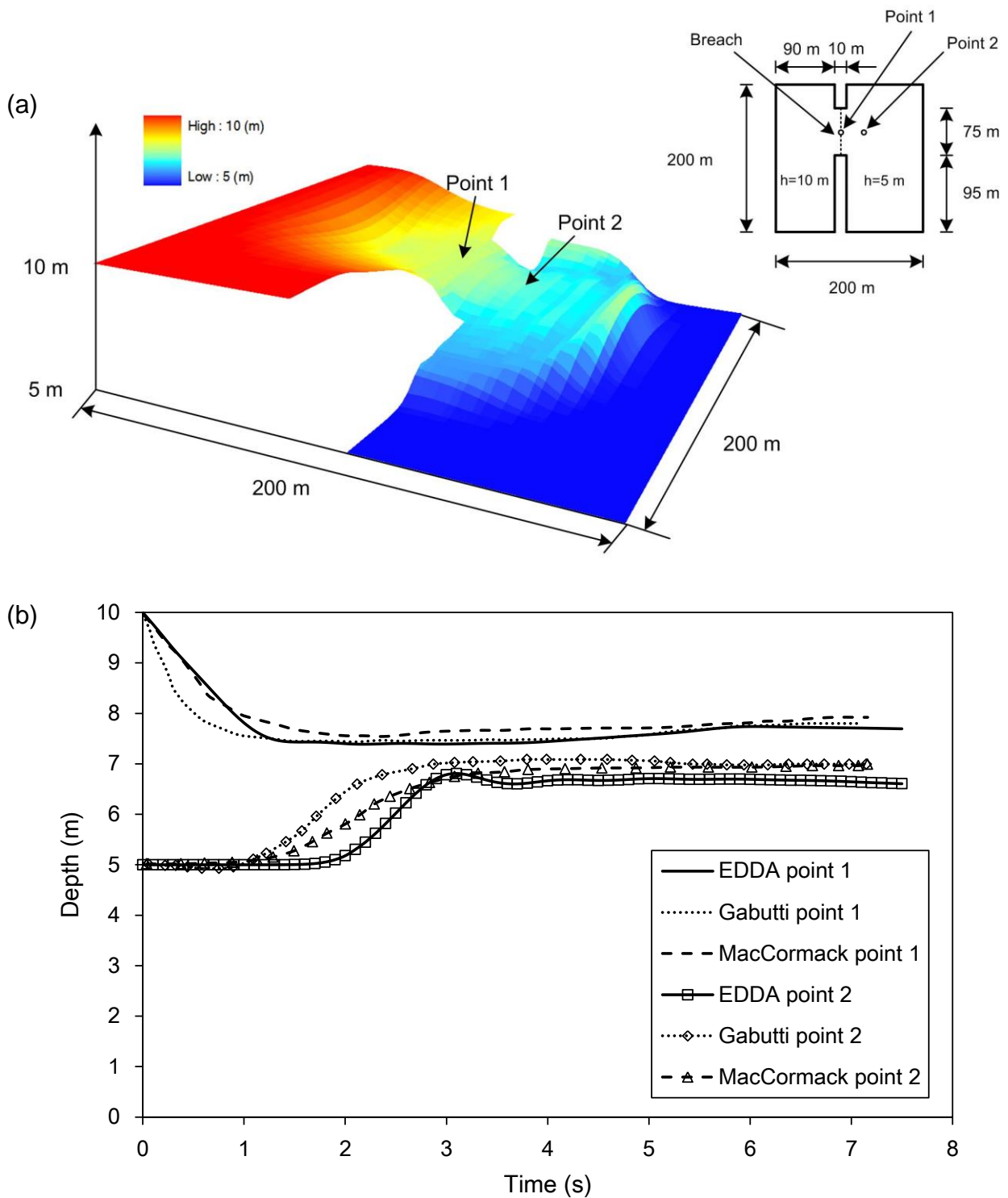


Figure 8. Numerical solutions in Test 2: (a) water depth at 7.1 s after the dam breaches computed by EDDA; (b) comparison of the computed water depths at selected points using EDDA developed in this study and two numerical schemes reported by Fennema and Hanif Chaudhry (1987).

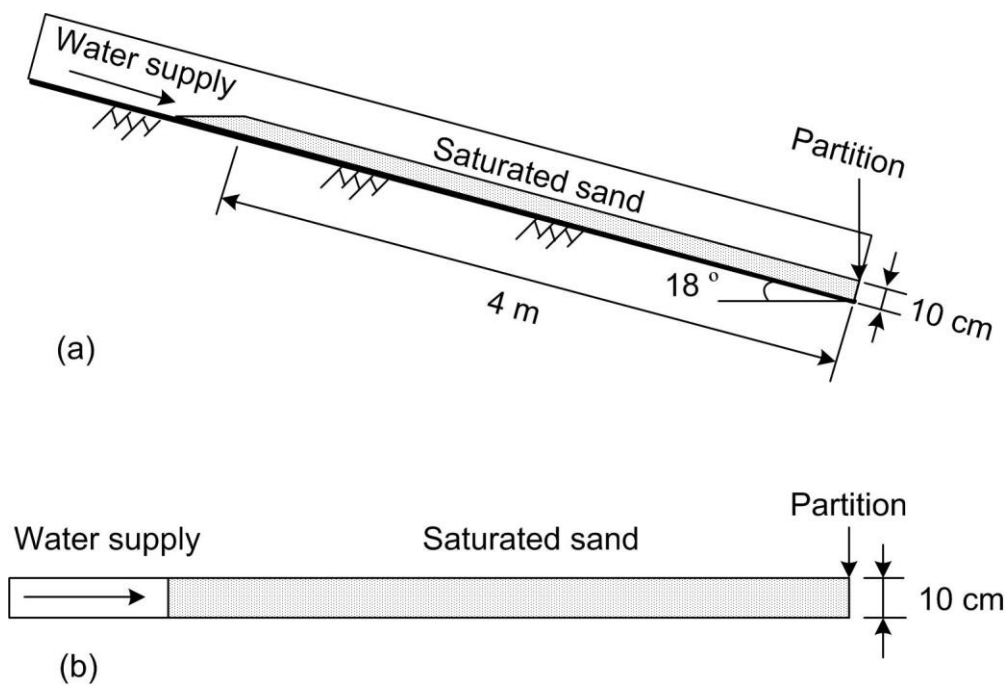


Figure 9. Experiment setup in Test 3: (a) side view; (b) top view.

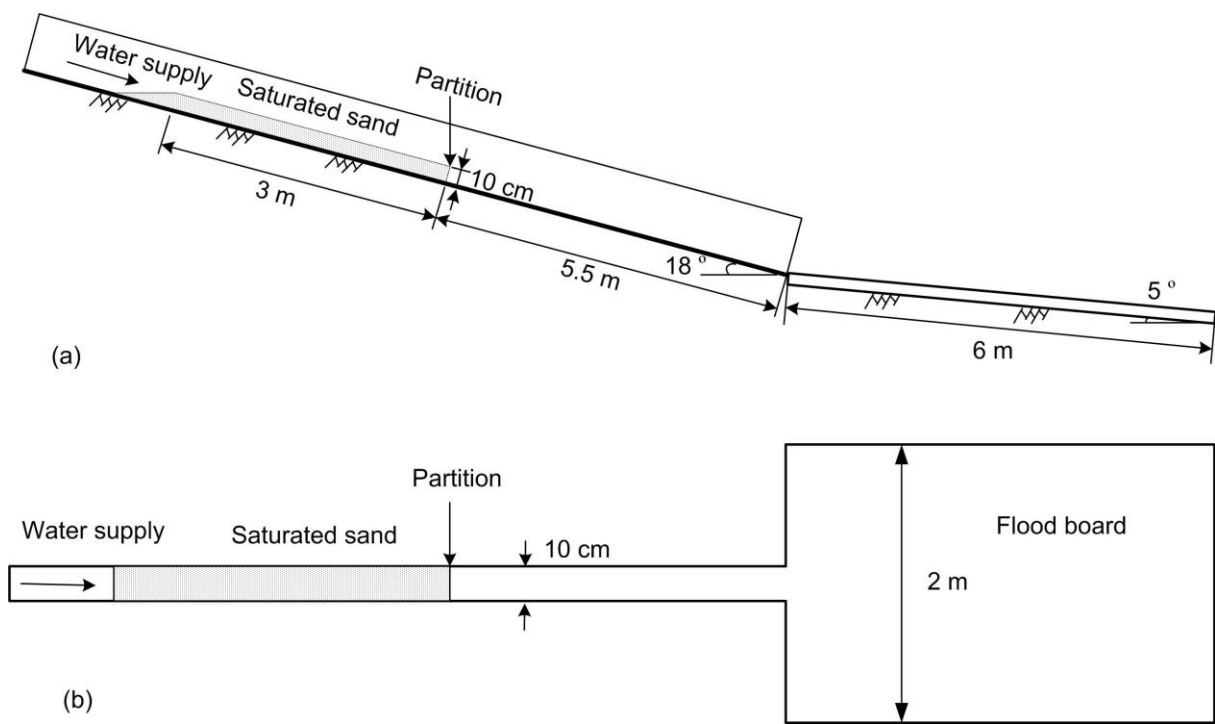


Figure 10. Experiment setup in Test 4: (a) side view; (b) top view.

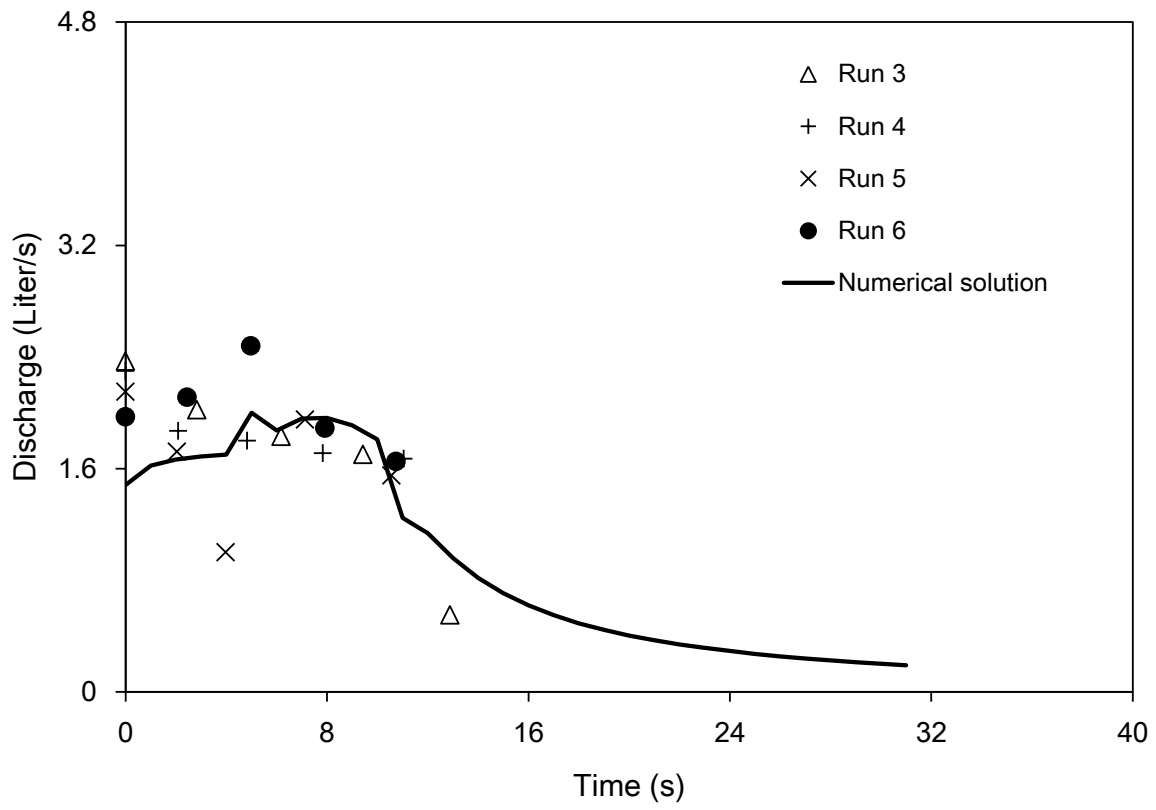


Figure 11. Comparison of discharge hydrographs at the downstream end of the flume in Test 4.

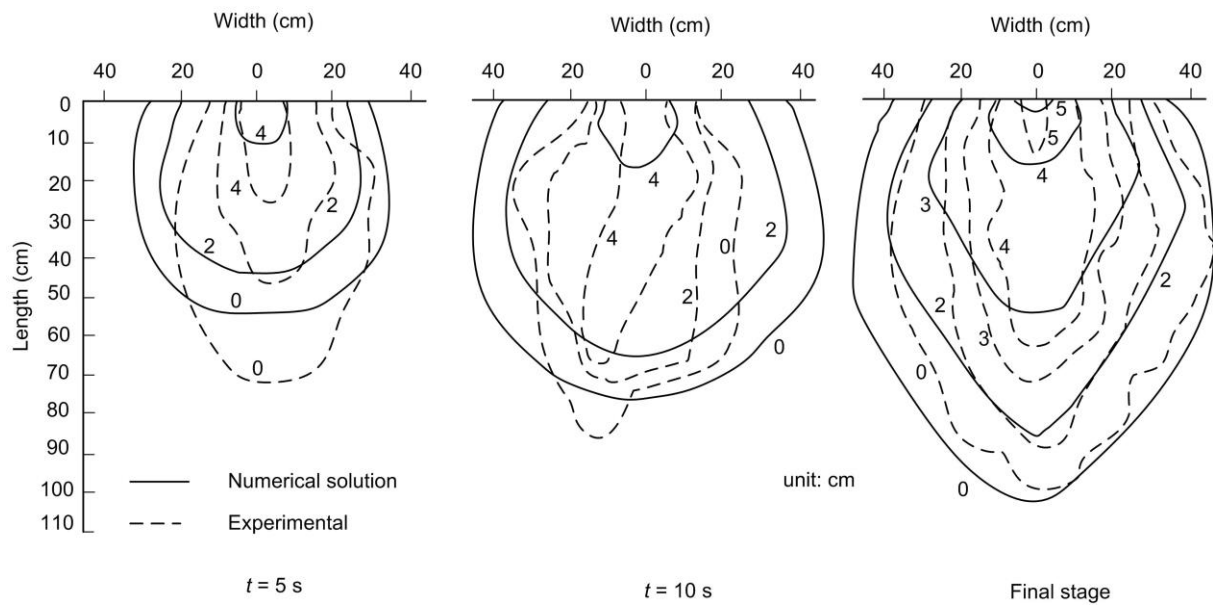


Figure 12. Comparison of the time-varying geometry and elevations of the debris fan in Test 4 from the numerical solution and the experimental tests.

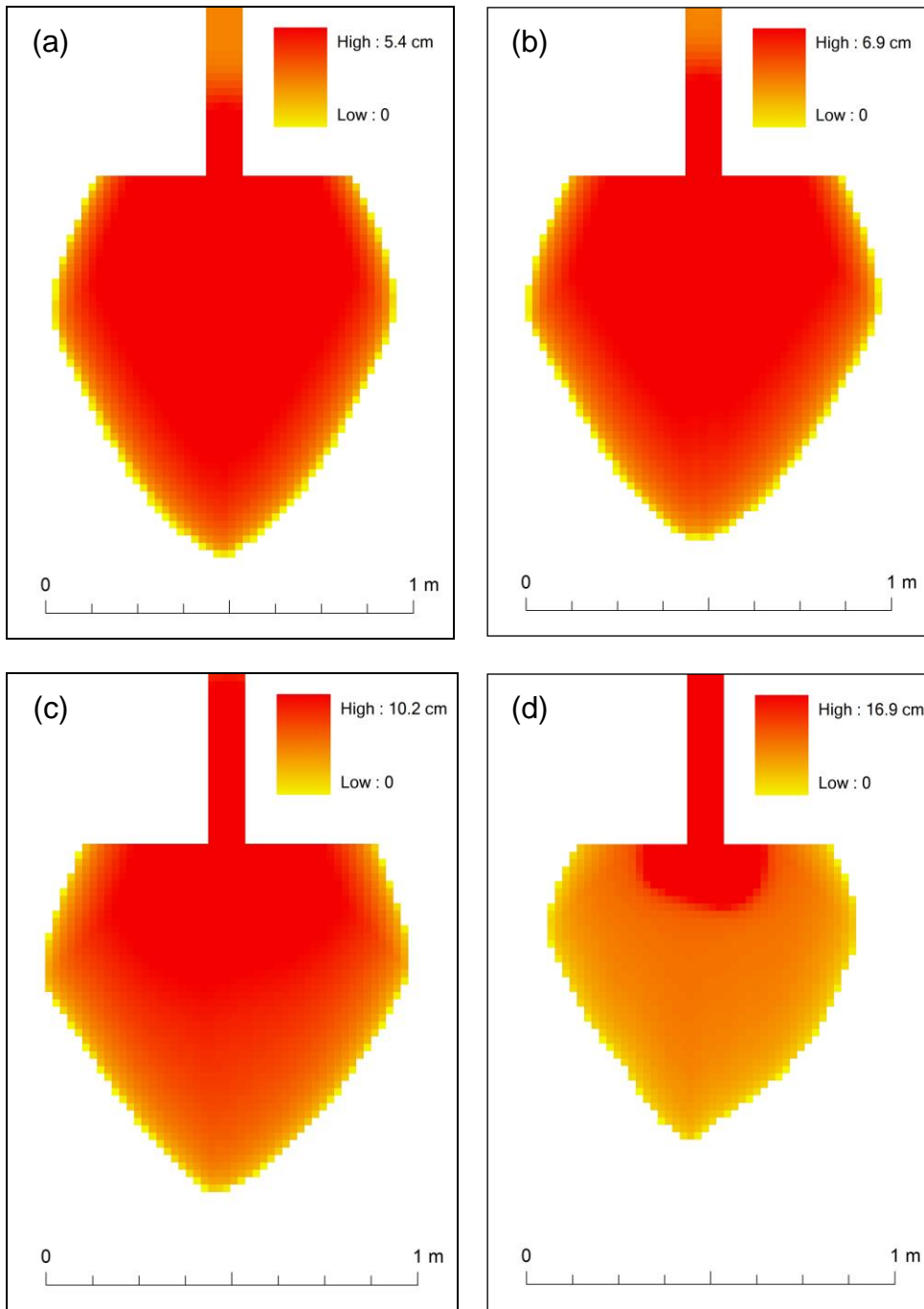


Figure 13. Debris fans at final stage considering different numerical constants for deposition rate: (a) δ_d is 0.03; (b) δ_d is 0.05; (c) δ_d is 0.1; (d) δ_d is 0.5.

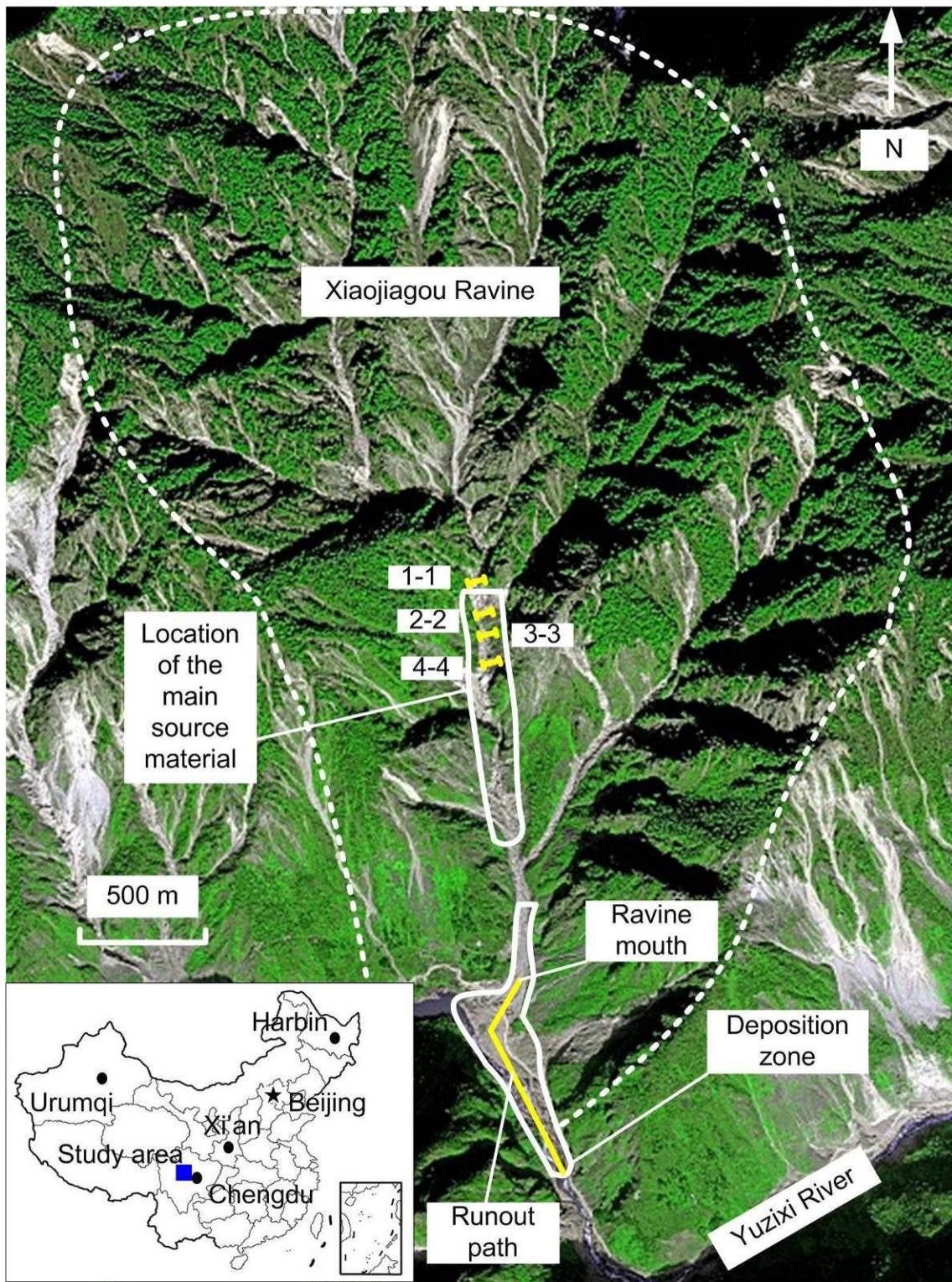


Figure 14. Location of the study area and a satellite image shortly after the Xiaojiagou debris flow.

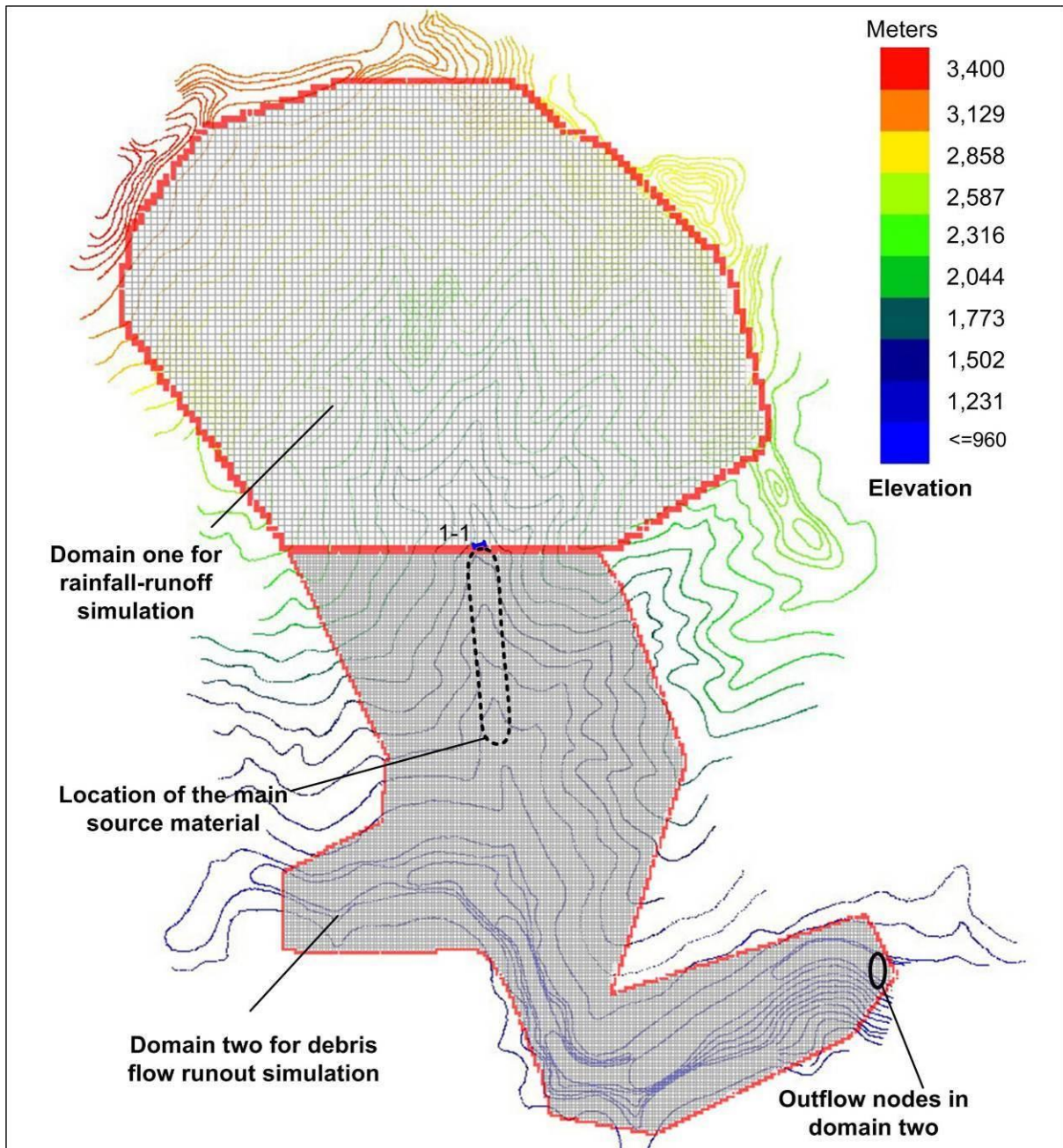


Figure 15. Grid system for rainfall runoff simulation and debris flow runout simulation.

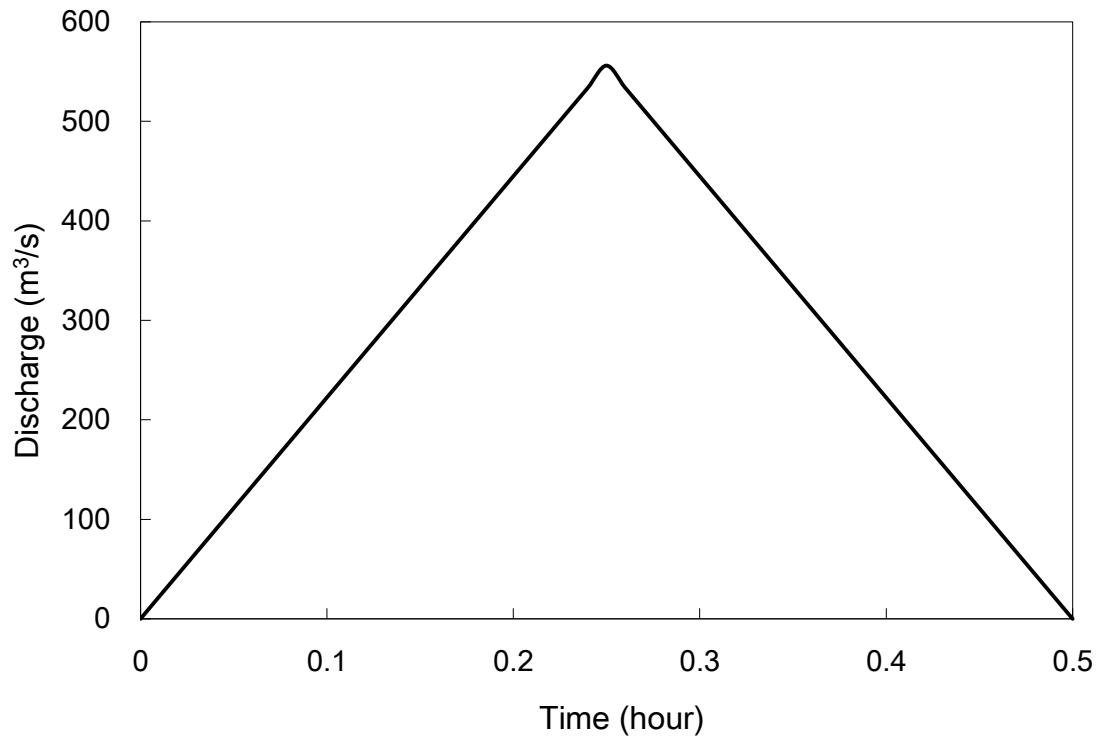


Figure 16. Surface water inflow hydrograph for debris flow runout simulation.

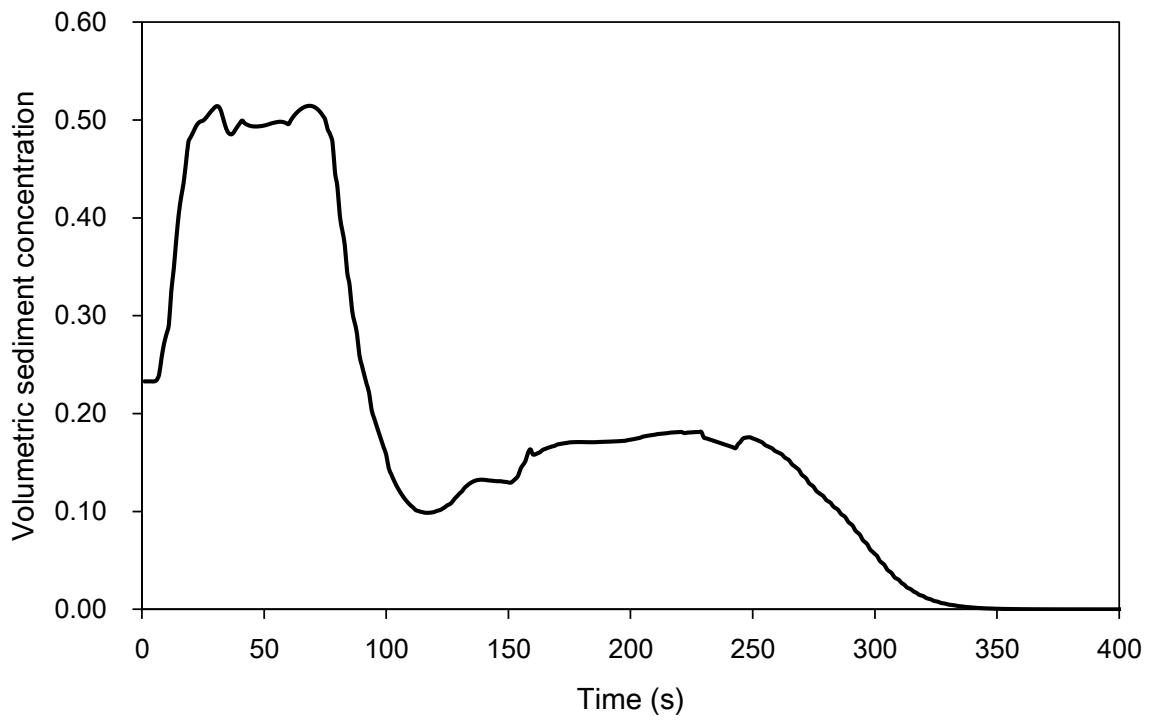


Figure 17. Change of volumetric sediment concentration at Section 3-3 in Fig. 14.

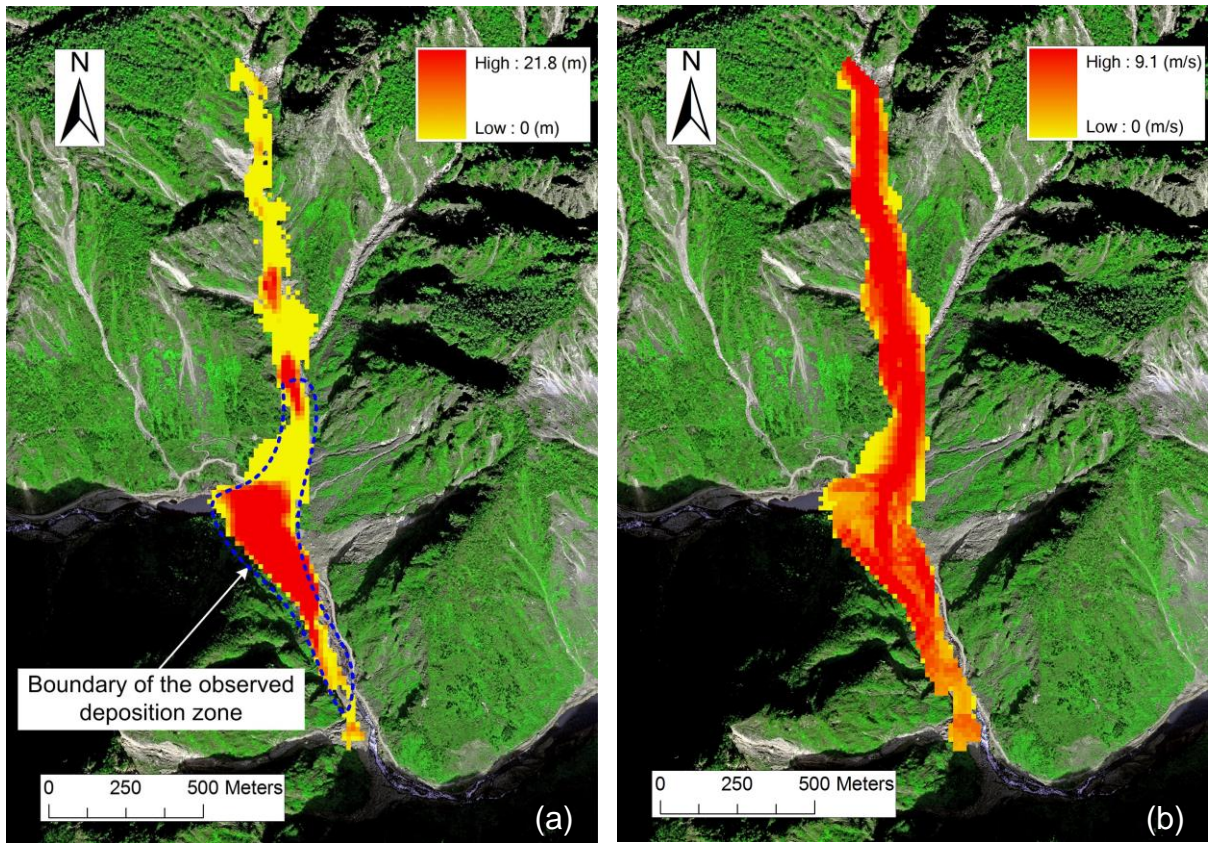


Figure 18. Simulation results of the Xiaojiagou debris flow: (a) final shape and depth of the deposition zone; (b) the maximum flow velocity.